Sequence analysis of ctDNA in NHL to monitor tumour progression and evolution

by

Stephen Yu

B.Sc., Simon Fraser University, 2013

Thesis Submitted in Partial Fulfillment of the

Requirements for the Degree of

Master of Science

in the

Department of Molecular Biology and Biochemistry

Faculty of Science

© Stephen Yu 2018

SIMON FRASER UNIVERSITY

Spring 2018

Approval

Name:	**Stephen Yu**
Degree:	**Master of Science**
Title:	**Sequence analysis of ctDNA in NHL to monitor tumour progression and evolution**
Examining Committee:	**Chair:** **Dr. Christopher Beh**
	Associate Professor

Dr. Ryan Morin
Senior Supervisor
Assistant Professor

Dr. Robert Holt
Supervisor
Professor

Dr. Christian Steidl
Supervisor
Associate Professor

Dr. Sharon Gorski
Internal Examiner
Professor

Date Defended/Approved: April 09, 2018

Ethics Statement

The author, whose name appears on the title page of this work, has obtained, for the research described in this work, either:

a.   human research ethics approval from the Simon Fraser University Office of Research Ethics

or

b.   advance approval of the animal care protocol from the University Animal Care Committee of Simon Fraser University

or has conducted the research

c.   as a co-investigator, collaborator, or research assistant in a research project approved in advance.

A copy of the approval letter has been filed with the Theses Office of the University Library at the time of submission of this thesis or project.

The original application for approval and letter of approval are filed with the relevant offices. Inquiries may be directed to those authorities.

<div align="right">
Simon Fraser University Library
Burnaby, British Columbia, Canada

Update Spring 2016
</div>

Abstract

NHL (non-Hodgkin lymphoma) is the fifth and sixth most prevalent cancer in Canada diagnosed annually among men and women respectively. With current conventional treatment, the five year survival rate is 67%. However, continued observations post-treatment are needed due to the risk of patient relapse. Liquid biopsies provide an effective, non-invasive means for such observations. Here, we evaluated the efficacy and utility of circulating tumour DNA (ctDNA) in relapsed patients with NHL. We detected ctDNA in at least one plasma sample from 90.9% of patients tested. We showed a significant increase in ctDNA was associated with a lack of treatment response. We demonstrate the utility of ctDNA to facilitate genetic characterization and direct observation of tumour heterogeneity and evolution. These results support the utility of ctDNA as a biomarker for tumour progression and as a substrate to study the genetic dynamics of NHL tumours over the course of treatment.

Keywords: cancer; genomics; circulating tumour DNA; biomarkers; next-generation sequencing; single molecule identification

For the countless survivors of cancer,

your perseverance through hardship is awe-inspiring,

and fuels my motivation to improve.

Acknowledgements

Table of Contents

List of Tables

List of Figures

List of Acronyms/Abbreviations

ABC DLBCL	Activated B-cell-like diffuse large B-cell lymphoma
BCCA	BC Cancer Agency
BCLU	B-cell lymphoma unclassified
CA125	Cancer antigen 125
CA15-3	Cancer antigen 15-3
CEA	Carcinoembryonic antigen
cfDNA	Cell free DNA
ChIP-Seq	Chromatin immunoprecipitation sequencing
CI	Confidence interval
COM	Composite lymphoma
CPC	Common progenitor cell
CSC	Cancer stem cell
CTC	Circulating tumour cells
ctDNA	Circulating tumour DNA
DA-EPOCH-R	Dose adjusted etoposide, doxorubicin, cyclophosphamide, vincristine, prednisone and rituximab
DLBCL	Diffuse large B-cell lymphoma
FL	Follicular lymphoma
GCB DLBCL	Germinal-center B-cell-like diffuse large B-cell lymphoma
GE	Genome equivalents
HDACi	Histone deacetylase inhibitors
HMW DNA	High molecular weight DNA
HSC	Hematopoietic stem cell
IGH	Immunoglobulin heavy chain
Indel	Insertions and deletions
ITH	Intra-tumour heterogeneity
JGH	Jewish General Hospital
LOD	Limit of detection
MCL	Mantle cell lymphoma
NHL	Non-Hodgkin lymphoma
NPV	Negative predictive value
PPV	Positive predictive value

ProDuSe	Process duplex sequencing
PSA	Prostate-specific antigen
R-ACVBP	Rituximab, doxorubicin, cyclophosphamide, vindesine, bleomycin and prednisone
R-CHOP	Rituximab, cyclophosphamide, doxorubicin, vincristine and prednisone
rrDLBCL	Relapsed or refractory diffuse large B-cell lymphoma
SBS	Sequence by synthesis
SNV	Single nucleotide variants
tFL	Transformed follicular lymphoma
VAF	Variant allele fraction
WES	Whole exome sequencing
WGS	Whole genome sequencing

Chapter 1.

Introduction

1.1. Cancer

1.1.1. Impact of cancer on the Canadian population

Cancer is the leading cause of death in Canada, responsible for 30% of all deaths[1]. Men are expected to have a 49% chance of developing cancer in their lifetime, which is slightly higher than women, having a 45% probability. Incidence of cancer (per capita cancer diagnosis rate) has been steadily increasing over the past decade to an estimated 206,200 new cases in 2017, resulting in an estimated number of 80,800 deaths due to ineffective therapies. Despite an increase in incidence, the ratio of deaths to new cases in 2017 has significantly decreased to 39% whereas in 2005 the proportion of new cases expected to succumb to the disease was 47%[2]. The decrease in mortality is a direct result of improvements in earlier cancer detection, more accurate diagnosis and more precise and diverse forms of treatment. Although great strides have been made towards improving the chances of survival, cancer still remains a disease with unacceptably high mortality given its incidence, with one in four Canadians expected to die from some form of cancer.

Cancer progresses from early events in which normal somatic cells acquire somatic mutations that allow them to divide uncontrollably. The accumulation of these cells can form a benign mass or malignant tumour, evidence of which have been observed as far back as 400 B.C., when the Greek physician Hippocrates described these as "karkinos", the Greek word for crab (or its Latin equivalent, cancer)[3]. By the start of the 18th century, many incorrect theories were formulated to explain the cause of cancer, including physical trauma and external parasites. In 1761, John Hill reported tobacco smoke as a likely cause of cancer (i.e. carcinogen)[4], furthering the belief in external factors as the root cause of cancer. Although the environmental impact of tobacco smoke was indeed proven to be a contributing factor, DNA damage resulting from exposure to carcinogens had not yet been appreciated as the underlying cause. It was not until the start of the 20th century, when scientists observed evidence that this

abnormal behaviour resulted from genetic alterations that had accumulated within the cells leading to the tumour. In 1902, Theodor Boveri performed a variety of cytological experiments on sea urchin nuclei and concluded that some chromosomal abnormalities can impair normal cellular function without affecting viability, thereby resulting in abnormal development[5]. The understanding that heritable changes to the chromosome or DNA (i.e. mutations) does not necessarily ensure cell death, led to further studies on the effects of DNA damage. In 1915, Katsusaburo Yamagiwa and Koichi Ichikawa applied coal tar to rabbit skin[6], which was the first documented case of experimentally inducing cancer through a carcinogen, adding credence to the role of carcinogens in cancer.   Finally, in 1960, Peter Nowell and David Hungerford identified a characteristically small chromosome in a tumour cell of two patients with chronic myeloid leukemia[7], providing strong evidence to support Boveri's conclusions.

1.1.2. Tumourigenesis

A healthy cell undergoes a cycle of growth and death naturally. However, a healthy cell can acquire a set of genetic differences from its parental cell and additional mutations during its lifetime, each of which are termed somatic mutations[8]. All cancer cells contain somatic mutations that are absent from most normal cells in a patient collectively referred to as the "germline"[9]. Somatic mutations that can be readily identified in cancer genomes include single nucleotide variants (SNVs), insertions and deletions (hereafter referred to as indels), structural rearrangements, and copy number alterations[10]. Chemical carcinogens such as tobacco smoke or other DNA damaging agents such as UV light can induce changes which, if unrepaired, are propagated as somatic mutations[11]. Somatic mutations affecting genes that confer a growth advantage to the cell are termed "driver" mutations[12]. Cells that acquire a handful of driver mutations, mostly affecting genes related to cell growth, cell division or regulation, will result in uncontrolled clonal expansion from a single, abnormal cell to form a proliferating mass of cells (i.e. tumourigenesis)[13]. The majority of somatic mutations observed in cancer genomes are not drivers. These "passenger" mutations are not subject to selection or involved in initiation of tumourigenesis[14]. Tumours can appropriate blood and nutrient supplies to continue to grow and potentially spread (metastasize) to another part of the body.

A gene containing a driver mutation that causes gain-of-function in a cell resulting in a selective growth advantage is termed an oncogene. Conversely, genes containing loss-of-function mutations that promote tumourigenesis are termed tumour suppressor genes[15]. Unlike oncogenes, tumour suppressor genes may be affected by inherited germline mutations and driver mutations. This distinction was first proposed by Alfred Knudson as the "two-hit hypothesis" for patients with retinoblastoma[16]. In this model, patients with a germline mutation affecting one allele of a gene requiring biallelic mutation (in this case, *RB1*) has a single "hit" and only requires another driver mutation to affect the second allele to cause loss of *RB1* function resulting in tumourigenesis. This model does not encompass all tumour suppressors. Counter to this model, specific single amino acid substitutions of the tumour suppressor *TP53* can block function of the normal p53 protein. Such mutations are referred to as "dominant negative", and pose an exception to the two-hit model of tumour suppressors.

1.1.3. Tumour heterogeneity and evolution

Cancer progression is a Darwinian evolutionary process at the level of cellular populations wherein the fitness of individual cells leads to survival and allows further mutation and selection[17]. One model of this process involves a sub-population of slowly replicating cells known as cancer stem cells (CSC). This was first discovered in acute myeloid leukemia in which there was evidence of a CSC that possessed similar proliferative and self-renewal capacities as a hematopoietic stem cell (HSC) and was capable of initiating tumourigenesis[18]. The cancer stem cell model suggest tumour cells expand through a hierarchy whereby the CSCs can undergo asymmetric division that can repopulate the CSC pool and yield terminally differentiated cells that are non-tumourigenic but can still contribute to tumour size. In another model, all tumour cells are equipotent and will stochastically self-renew into new CSCs or become terminally differentiated cells[19]. These modes of evolution are frequently used to explain tumour growth and heterogeneity. Although there have been cases where CSCs were identified in lymphoma[20,21], there is still controversy over whether both models are relevant to lymphoma[22]. Recent studies suggest a shared model involving both hierarchical and stochastic concepts is a more likely explanation for tumour heterogeneity[22].

All tumour cells contain mutations inherited from an ancestral common progenitor cell (CPC)[23]. The CPCs embody the "trunk" of a phylogenetic tree that represents the

clonal structure of a tumour, and "branches" represent differentiated cells derived from the founding CPCs[24]. Tumour cells can undergo clonal expansion to produce genetically identical tumour cells referred to as clones, and the mutations contained within are referred to as clonal mutations. Expectedly, clonal mutations are found in the vast majority of tumour cells. Clones can gain additional mutations which may confer a selective, phenotypic advantage and expand within a tumour microenvironoment[25,26]. These outgrowths are referred to as sub-clones, and continued evolution of sub-clones lead to a varied population of cells wherein the genetic and phenotypic composition of the tumour can be heterogeneous and diverse.

There are four competing models proposed to describe evolution of CPCs into sub-clones: linear evolution, branched evolution, neutral evolution and punctuated evolution[27]. Linear evolution posits new driver mutations provide a selective advantage to a single clone that outcompetes all other clones, resulting in a dominant clone sequentially gaining mutations fueling tumour growth, as evidenced in colorectal cancer[28]. Branched evolution suggests sub-clones diverge from a CPC and evolve in parallel due to shared fitness. This evolution results in gradual accumulation of new driver mutations, leading to clonal expansion and evolution within the tumour mass, and has been shown in various cancers including leukemia[29]. Neutral evolution is similar to branched evolution, however it is suggested that there is no selection or fitness changes within the tumour microenvironment. This model assumes random mutations are accumulated over time, resulting in tumour heterogeneity. There is weak support for this model. Punctuated evolution suggests the majority of genomic aberrations occur in short bursts of time, particularly during the early stages of tumour progression. Intra-tumour heterogeneity (ITH), which refers to the distinct clonal and sub-clonal compositions within one tumour mass, must be very high at this stage, resulting in expansion of a few dominant clones to form the tumour mass. One common theme among these four models is the presence of sub-clonal mutations, specifically sub-clonal driver mutations, which can provide a suitable target for studying tumour heterogeneity and understanding tumour evolution[30].

Studies have shown the degree of ITH can be highly diverse across many cancer types, and that the prevalence of sub-clonal mutations can be used to infer a tumour's phylogeny[31]. Importantly, ITH can be dynamic as sub-clonal populations compete for resources in the tumour microenvironment during the course of a disease. ITH can

change temporally, especially during treatment. Studying ITH through analysis of sub-clonal mutations can provide predictive or prognostic biomarker strategies, which has implications towards therapeutic outcome[31].

Similar to ITH, inter-tumour heterogeneity refers to the genetic and phenotypic variation between clones and sub-clones between tumours found at physically distant metastatic sites in a patient, and is often referred to as spatial heterogeneity. Inter-tumour heterogeneity is exacerbated by the different micro-environments in the body, which may provide a selective advantage for certain sub-clonal tumour populations. Interestingly, studies have found histologically similar tumours from different parts of the same organ exhibit different responses to therapy due to the underlying genetic differences from inter-tumour heterogeneity[32]. Genomic instability of tumour clones, resulting in the emergence of different sub-clones, lead to the increased level of intra- and inter-tumour heterogeneity in patients[33]. Notably, tumour heterogeneity can hinder accurate diagnosis and effective treatment for certain cancers[32]. Regardless, studies on tumour heterogeneity can provide opportunity for rapid response to therapy and ultimately allow evolution of drug resistance.

1.2. Non-Hodgkin Lymphoma

Non-Hodgkin lymphoma (NHL) is a diverse group of cancers arising from mature B- or T-cells and typically manifest as solid tumours in the lymph nodes and other lymphoid tissues such as the bone marrow, thymus and spleen. NHLs originate from white blood cells that have acquired a sufficient set of somatic mutations affecting genes that lead to clonal expansion and ultimately tumourigenesis[34]. It is estimated that 8,300 Canadians will be diagnosed with NHL in 2017[1]. NHLs account for 90% of all lymphomas, while the other 10% is referred to as classical Hodgkin's lymphoma. Hodgkin's lymphoma is recognized by the presence of the Reed-Sternberg cell, an easily identified malignant cell that can be multinucleated and is larger than the B-cells from which it is thought to originate[35].

1.2.1. Diffuse large B-cell lymphoma

The most common type of NHL is diffuse large B-cell lymphoma (DLBCL), an aggressive lymphoma originating from B-cell lymphocytes. DLBCLs account for

approximately 31% of all NHL[36], occurring primarily in older individuals with a median age of 70 years[37]. There are two molecular subgroups of DLBCL, namely the germinal-center B-cell-like (GCB) and activated B-cell-like (ABC) varieties. Both are characterized by unique gene-expression profiles but are histologically indistinguishable[38,39]. Based on gene expression profiles, GCB DLBCLs resemble B-cells residing in the germinal center of a lymph node or spleen and are thought to have originated from this cell type[40]. The germinal center is an area where naïve B-cells undergo clonal expansion and somatic hypermutation to become mature B-cells. ABC DLBCLs are thought to derive from activated B-cells, which are B-cells poised to exit the germinal center destined to become antibody-secreting plasma cells[41]. ABC DLBCL is the more aggressive subgroup with a generally worse prognosis on standard chemotherapy (such as R-CHOP)[42].

Extensive research has been performed to identify frequently mutated genes in DLBCL. The histone methyltransferase *EZH2* was associated with only GCB DLBCL, observed in 21.7% cases[43]. Further studies showed other histone-modifying genes were also associated with DLBCL, for example *MEF2B* and *MLL2*[44]. Additionally, inactivation of acetyltransferase genes such as *CREBBP* and *EP300* have been reported[45].

1.2.2. Follicular lymphoma

Follicular lymphoma (FL) is the second most common NHL, accounting for approximately 20% of cases[46]. FL is slow-growing and indolent compared to DLBCL, with a wide range of survival. It is typically incurable with current chemotherapy treatment. Similar to GCB DLBCL, malignant cells in FL originate from germinal center B-cells[41]. The translocation t(14;18)(q32;q21), which affects the *BCL2* gene and the immunoglobulin heavy chain locus (IGH), is observed in 90% of FL cases resulting in constitutive overexpression of BCL2 protein[47]. Notably, a recent study reported 89% of FL cases showed mutations in the methyltransferase *MLL2*[44]. This study also reported frequent mutations in other histone-modifying genes such as *MEF2B*, *CREBBP* and *EP300* in FL. Additional genetic changes associated with FL include *EZH2* mutations[43], *TP53* mutations[48], and other *BCL2* and *BCL6* mutations[49].

FL can undergo a histologic transformation to a more aggressive lymphoma, referred to as transformed FL (tFL), that resembles DLBCL and the outcome and

6

survival of patients with tFL is poor[50]. Cases of DLBCL that are diagnosed without prior evidence of FL are commonly described as *de novo* DLBCL to differentiate them from this more aggressive disease. The aetiology of tFL remains unclear but it is important to consider this disease in the context of DLBCL because many clinical trials for new therapies include patients with tFL. There is hope that individualized treatment approaches may improve overall survival in tFL[51].

1.2.3. Treatment and survival

Conventional treatment, namely R-CHOP (rituximab, cyclophosphamide, doxorubicin, vincristine, and prednisone), successfully cures a substantial proportion of patients[52], however up to 40% of patients with DLBCL[53] and tFL[54] are not cured with standard chemoimmunotherapy or high dose therapy and autologous stem cell transplantation. Rituximab is a monoclonal antibody that binds the CD20 surface antigen on B-cells[55], and triggers natural killer cell mediated antibody-dependent cellular cytotoxicity to destroy the B-cell[56]. Cyclophosphamide acts as an alkylating agent, forming cross-links to damage DNA[57]. Doxorubicin acts as an intercalating agent, inserting itself between bases to damage DNA, and can bind certain enzymes to produce cytotoxic effects[58]. Vincristine binds partly to tubulin protein, inhibiting separation of chromosomes during mitosis[59]. Prednisone is a corticosteroid used to suppress the immune system. The effects of these drugs lead to apoptosis, the process of programmed cell death.

Development of more effective chemotherapy options have led to such therapies as R-ACVBP (rituximab, doxorubicin, cyclophosphamide, vindesine, bleomycin and prednisone)[60] and DA-EPOCH-R (dose adjusted etoposide, doxorubicin, cyclophosphamide, vincristine, prednisone and rituximab)[61]. Vindesine has similar effects to vincristine, preventing cell division from occurring by disrupting tubulin, and bleomycin acts by inducing DNA strand breaks leading to apoptosis. Etoposide targets topoisomerases used to re-ligate DNA strands after unwinding during DNA replication and transcription, which results in DNA strand breaks[62]. These highly effective chemotherapies, though similar to R-CHOP, are only used for patients with certain molecular subtypes, such as using R-ACVBP to treat poor-prognosis aggressive NHLs[60,63].

Side-effects for chemotherapy treatment are numerous, including fatigue, vomiting, constipation, and diarrhea. Notably, patients may develop cytopenia[64], a general reduction in mature blood cells. Reduction can be specific to certain cells, such as a reduction in red blood cells (anemia[65]), white blood cells (neutropenia[66]), or platelets (thrombocytopenia[67]). A reduction in all three is referred to as pancytopenia[68]. Harmful side-effects of chemotherapy need to be considered when choosing treatment options for patients, and it is important to determine if treatment is failing, so the patient can be taken off treatment to prevent unnecessary complications. Personalized treatment strategies is a possible solution, however there is a need for robust, cost-effective methods to monitor changes during treatment to enable such personalized strategies.

One such therapeutic class includes histone deacetylase inhibitors (HDACi), potentially applicable in DLBCL patients due to the high frequency of mutations in histone-modifying genes. HDACi cause epigenetic changes by increasing acetylation of histones and non-histone proteins. Mutations in histone-modifying genes change the epigenetic landscape and chromatin structure, resulting in transcriptional changes. Panobinostat, a novel HDACi, is currently being used in phase II and III clinical trials[69]. EZH2 inhibitors are also used in targeted therapy for patients with GCB DLBCL. These inhibitors, such as GSK126[70] and EI1[71], inhibit this histone methyltransferase resulting in decreased proliferation and apoptosis in DLBCL cell lines and xenograft mouse models.

1.3. Biomarkers and Disease Monitoring in NHL

Guided by specific clinical symptoms and the presence of certain protein markers in the blood, suspected lymphoma can only be definitively diagnosed using tumour tissue biopsies[72]. Tissue biopsies have also been the source of genetic material for genetic characterization. Non-invasive approaches to measure tumour burden are desirable because they can be more frequently performed during the course of treatment. In NHL patients, clinicians use non-invasive imaging techniques such as CT (computed tomography) scans or PET (positron emission tomography) scans to monitor disease and detect relapse[73]. CT scan combines multi-angle X-rays from a specific site in the body to produce cross-sectional images, which allow assessment of organ (and tumour) size[74]. PET scan is an imaging technique that detects gamma rays emitted by a positron emitting (radiolabel) tracer injected into the patient[74]. The use of PET scans with the tracer FDG (2-fluoro-2-deoxy-D-glucose), a glucose analog that is radiolabeled with

the positron emitter fluorine-18, has been effective in staging and monitoring of patients with NHL[75]. Size is typically reported as the sum of the products of the perpendicular diameters of a lesion (SPD)[76]. PET scans are less detailed than CT scans, especially in cases with low or variable FDG uptake, however, current methods for determining disease stage and for disease monitoring rely on a combination of PET/CT scans[76]. Using either method, the size and changes in size of lesions are commonly used to identify disease progression or response to therapy[77].

Frequent monitoring with these imaging techniques are costly and time-consuming, and may result in complications such as secondary primary malignancies that form due to radiation exposure[78]. Additionally, studies have shown CT scans play only a small role in detecting relapse in patients[79], and that since relapse after initial remission is rare, repeat scans may not result in improved survival[80]. Because only a minority of patients will relapse on therapy, routine imaging scans post-treatment are not informative in most cases. Clinicians manage dose, scan length, and frequency of scans to prevent unnecessary levels of radiation exposure[81].

In the follow-up of patients, clinicians use a variety of tests including physical examinations, blood tests, and biochemical profiling, in addition to CT or PET-CT scans[82]. Biochemical profiling utilize specific biomarkers for monitoring disease, and are favored to avoid performing frequent CT scans[78]. Serum lactate dehydrogenase (LDH) is a blood protein biomarker that, when elevated, can imply a worse prognosis and may increase at relapse[83,84]. In contrast, LDH levels in the normal range are associated with better response to therapy and longer survival[85], thus LDH is a useful prognostic biomarker.

Owing to these issues, it is desirable to identify markers that could be measured non-invasively to facilitate more frequent monitoring of patients as an adjunct to existing methods such as tumour biopsies or CT scans. Currently, researchers utilize a multi-phase system for screening potential biomarkers[86]. This starts with preclinical exploratory studies to identify specific characteristics unique to tumour cells that may lead to development of clinical tests to utilize such characteristics. Typically, this involves the identification of genes that are differentially expressed in the tumour or contain somatic mutations that are unique to the tumour cell population. Next, an assay that measures the biomarker must be implemented and its potential to differentiate between

samples from patients with and without the disease is assessed. This aims to estimate the accuracy and true and false positive rates of a potential clinical test. After a test has been developed, retrospective longitudinal studies with appropriate clinical samples can be used to assess the utility of the test in measuring a specific clinical parameter. This is then separately evaluated in a prospective setting. Ultimately, the biomarker and the associated clinical test should be shown to result in an overall benefit in the treatment or diagnosis of the disease. For this study, I set out to implement some methods to detect and measure circulating tumour DNA in NHL patients and explore its potential utility as a biomarker for monitoring treatment response.

1.4. Circulating Tumour DNA

Extracellular DNA that is circulating in the blood plasma is termed cell free DNA (cfDNA). Circulating tumour DNA (ctDNA) specifically refers to cfDNA shed from the tumour cells into the blood stream through processes such as apoptosis[87]. Typically, ctDNA and cfDNA fragments range between 150 to 180 bp[88], roughly the length of DNA wrapped around a mononucleosome, although multiples of this length are also observed. Every tumour cell contains somatic mutations that are, by definition, absent from most of the normal cells in the body, and we can assay for these somatic mutations to differentiate ctDNA molecules from cfDNA based on the presence of these mutations. Cancer patients are assumed to have higher cfDNA levels than healthy individuals, though this can widely vary between patients[89]. Although reports of abnormally high levels of cfDNA in cancer patients have been demonstrated since 1977[90], the utility of cfDNA as a predictive biomarker for disease has not been fully studied. Reliable detection of ctDNA may be challenging, as ctDNA comprises a small fraction of the total cfDNA[91]. Although the half-life of ctDNA is still a controversial subject, researchers have estimated it to be less than 2 hours[92]. This suggests that the abundance of ctDNA may afford a near real-time representation of tumour DNA release and genetic composition of those cells.

Circulating tumour cells (CTC) are tumour cells shed into the circulatory system from a primary tumour. CtDNA can be shed from CTCs[93], however, this is not the main source of ctDNA and patients may have high levels of ctDNA and no levels of CTCs. Surprisingly, CTCs are relatively rare, even in patients with metastatic cancer[94]. CTCs that do survive the vigorous passage of blood have been shown to stimulate invasion of

organs resulting in metastatic relapse[95]. Studies in metastatic breast cancer has demonstrated the utility of CTCs as a predictive biomarker of survival[94], though the presence of CTCs in a limited number of patients hinder its reliability. Other biomarkers typically used to monitor treatment response include protein antigens specific to certain cancer types, such as prostate-specific antigen (PSA), carcinoembryonic antigen (CEA), cancer antigen 15-3 (CA15-3) and cancer antigen 125 (CA125). PSA and CA125 are useful in monitoring patients with prostate and ovarian cancers, however they prove less useful in neoplasms such as lymphoma[96]. Additionally, there is a lack of reports for CEA biomarker tests in NHL. CA15-3 was shown to be detectable in NHL, but the success rate was less than 40% in one study[97].

The use of ctDNA as a potential biomarker, often known as liquid biopsies[98], has been posited as a non-invasive tool for frequently monitoring patient tumour burden[99]. This has been shown in DLBCL[100] and many other cancers[101,102]. Liquid biopsies are less invasive than solid tumour biopsies. One benefit of less invasive testing is a higher accepted frequency of testing. That is, patients can have blood drawn more frequently than undergoing surgery for biopsies[103]. When compared to a simple blood draw, tissue biopsies are associated with higher cost, morbidity and are far more invasive. At the onset of this project, little was known about the utility of ctDNA to capture tumour heterogeneity within a patient or to track clonal and sub-clonal mutations over time. The utility of liquid biopsies for detection of malignant disease was not well documented[104]. As such, further investigation into alternative methods of querying the tumour genome such as sequence analysis of ctDNA is warranted.

There is concern that tumour tissue biopsies can be spatially and temporally limited in their representation of the full genetic composition of a tumour (or tumours, in the case of disseminated disease). Tumour biopsies are usually taken from one location, and do not provide adequate representation of inter-tumour heterogeneity[105]. Furthermore, studies have shown single tumour biopsy samples are limited also by ITH, which lead to underestimation of the tumour genomic landscape[106]. Due to cost, invasiveness and tumour heterogeneity, reliance on tumour biopsies may present challenges towards personalized cancer diagnosis and treatment strategies.

1.5. Illumina Sequencing

DNA sequencing technology has steadily improved over the past two decades. More recently, development of next-generation sequencing techniques has allowed researchers to parallelize DNA sequencing experiments to provide a higher throughput of data at a much lower cost. This led to the application of next-generation sequencing techniques on frequent studies including whole genome re-sequencing to identify mutations, genomic mapping of structural rearrangements, RNA sequencing to determine differential gene expression, and genome-wide mapping of DNA-protein interactions (i.e. ChIP-Seq)[107].

Illumina sequencing is the most widely used next-generation sequencing technology[108]. We used Illumina sequencing platforms (most frequently, the Illumina MiSeq) for this project, because a large amount of data can be generated in a cost-effective manner. Illumina sequencing uses a "sequencing-by-synthesis" (SBS) method, where modified bases are added to a template strand, allowing for detection of incorporated bases. Briefly, indexed primers are added to DNA templates prepared for sequenced, referred to as a library. Indexed primers allow for sample identification when multiplexing and for annealing onto complementary oligonucleotides densely localized on an acrylamide-coated glass flow cell[109], a unique component of Illumina sequencing. DNA polymerases are used to synthesize complementary strands of the attached DNA templates to generate clusters of identical DNA fragments, in a process called "bridge amplification". The reverse strands are cleaved and washed away, leaving a cluster of forward strands ready for sequencing. Specialized nucleotide bases unique to Illumina are incorporated as SBS occurs. Each of the four nucleotide bases are labeled with a unique fluorescent label and have a "reversible" blocking group added to the 3'-OH[110,111]. Each cycle of sequencing involves the addition of the reversible terminator nucleotides which allows only a single-base incorporation to the DNA template. After acquisition of images relying on fluorescent labeling to identify the incorporated bases, the blocking group and florescent tag are chemical cleaved, allowing for the next cycle of sequencing to commence. After the predetermined number of cycles has been completed, clusters are re-generated to allow sequencing from the other adaptor and (typically) a third short read is generated to allow determination of the multiplexing index.

Illumina has three main platforms: The HiSeq series, the NextSeq series, and the MiSeq series. The HiSeq platforms are capable of the highest output overall, producing up to 3 billion reads in a single run[108]. One HiSeq run can take up to six days in high-output mode, typically used for whole genome or exome sequencing. For this project, we used the HiSeq 2500 for whole exome sequencing on tumour samples. The NextSeq platforms are much newer and provide a high level of output while reducing run time drastically. In high-output mode, the NextSeq 500 produces 400 million reads within one day[112]. For this project, we used the MiSeq for all experiments involving a targeted panel of mutations on plasma and tumour samples. The MiSeq can produce up to 25 million reads within one day, and importantly, produce the longest reads on any Illumina platform: 300 bases paired-end reads[113]. This is useful for reliable sequencing of DNA fragments longer than 150 bp.

1.6. Experimental Outline

This project was designed to establish the extent to which liquid biopsies can provide a non-invasive strategy for monitoring disease and explore (and implement) suitable techniques to assess this. With current technology, sensitive methods can be used to assay ctDNA in patients to track tumour progression. Currently, more data supporting the utility of ctDNA for monitoring disease progression is needed. Hopefully, these and future experiments can provide enough evidence to enable wider use of ctDNA analysis in clinical settings.

Here, I specifically sought to explore the utility of ctDNA as a biomarker in treatment response of patients with NHL. I set out to validate two different "personalized" sequencing-based methods to quantify ctDNA across multiple time points during treatment by querying sites of somatic mutation known to be present in the tumour of the patient. In doing so, I hope to identify whether these techniques could provide a sensitive, robust assay to monitor treatment response and to track specific genetic changes within the tumour. Ultimately, if validated, such an assay could allow monitoring of disease burden in a patient undergoing treatment without resorting to invasive tests. Such a result could be transformative to clinical care as it offers the potential to allow clinicians to detect a resurgence in tumour growth in patients otherwise showing no clinical signs of relapse.

As NHL is a genetically heterogeneous cancer, it is conceivable that multiple sub-clonal tumour cell populations exist in patients and these can have genetic differences that may affect their phenotype and fitness in the context of therapy. As tumour dynamics change during treatment, these sub-populations (or sub-clones) may decline or expand as a result of differential fitness. As the genetic differences between these populations could explain, in part, their differential response to treatment, it is crucial to develop a robust assay with applications for a wide range of mutation targets, which allow us to query for ctDNA from all sub-clones. It is also important to ensure this assay is cost-effective, so that it can be applied to many samples from a patient, allowing a more fine-grained analysis of tumour evolution.

This project is an exploratory study of the utility of ctDNA as a sensitive biomarker for monitoring disease progression and outgrowth of genetically distinct sub-clones during treatment. Similar to the initial phases of biomarker development, I will assess the capacity of ctDNA to detect disease, using potential target sites (genes) subjectively chosen to improve success. *Post hoc* analysis and additional testing is utilized in certain cases where our results differed from what we expected. There are two overarching objectives that outline this project, described in the next two subsections.

1.6.1. Objective 1: Determine the utility of ctDNA to inform on disease progression

In this project, I have utilized two main techniques for quantifying ctDNA in patients with NHL (detailed in Section 2.3). I assess these experiments for their sensitivity and robustness in detecting the presence (and level) of ctDNA. With multiple plasma samples drawn from different time points, I assess the potential to compare changes in ctDNA with disease progression in the patient. The results from this objective are discussed in Chapter 2.

Objective 1a: Determine efficacy of targeted amplicon sequencing for detecting ctDNA

The first assay specifically targets sites known to harbour somatic mutations in the patient and amplifies them *via* PCR using site-specific primers. First, using identified somatic mutations from whole genome or exome sequencing (WGS/WES) of tumour and matched normal samples from patients, I choose a suitable mutation affecting a

known lymphoma-associated gene (hereafter referred to as the target mutation). Next, I design primers targeting an appropriate length surrounding the mutation (less than 300 bp) and amplify the region by PCR. These primers have an added sequence to allow for a second, nested PCR using Illumina P5/P7 primers with barcodes for downstream identification. These rounds of PCR produce "amplicons", which are deeply sequenced (Illumina MiSeq).

I apply the patient-specific PCRs to DNA extracted from plasma samples taken at multiple time points and use this method (referred to as targeted amplicon sequencing) to identify reads representing the target mutation. One of the downsides to this method is the inability to target structural variations, especially if they drastically affect the size of the resulting amplicons. Here, I have limited the assay to targeting only SNVs, observed at a high frequency in tumour samples and affecting genes known to drive lymphomagenesis. This assay is "uniplex" in design such that each PCR is designed to detect one SNV per patient. At the start of these experiments, I decided that one properly selected SNV would represent the levels of ctDNA in each patient, hence why I had opted against multiplexing several target mutations.

Objective 1b: Determine efficacy of hybridization capture for detecting ctDNA

The second assay I employed involves using a set of biotinylated probes specific to gene regions known to be frequently mutated in NHL. These "capture" probes are hybridized to a library that has been constructed from cfDNA extracted from the plasma of patients. This enables enrichment of ctDNA and any DNA fragments from healthy cells (a component of cfDNA) representing the positions of interest that are fully or partially complementary to the probes. In comparison to amplicon sequencing, this allows for convenient massive multiplexing, as hundreds of these probes can be pooled together and used to enrich all sites from a single library in one tube. This has the potential for preparing specialized pools of probes personalized for one patient, which can provide greater enrichment of ctDNA. Additionally, we devised a variant of the duplex sequencing methodology[114,115] to provide error-suppression and aid in accurate detection of ctDNA. This addition involves custom adapters containing a set of degenerate nucleotides (molecular barcodes), unique to each strand of a DNA fragment providing single molecule identification during subsequent analysis.

The hybridization capture method is inherently superior to targeted amplicon sequencing in scalability. Hybridization capture provides us with a new level of time efficiency, allowing multiple target mutations from one patient to be detected concurrently. Cost-effectiveness is beneficial for these experiments, as we aim to test a series of plasma time points. If using a PCR-based approach, I would not be able to test as many regions in one targeted amplicon sequencing experiment and the design of personalized primers would have been onerous.

This objective involves the application of this approach to multiple plasma time points taken during the course of treatment. By keeping the probe pool consistent, I set out to look for any significant changes in ctDNA levels, and relate this data to tumour progression in the patient. To assess the potential clinical utility of this, I have access to clinical information on the patient regarding progression of their disease.

1.6.2. Objective 2: Assess tumour heterogeneity in patients through ctDNA analysis

The second objective of this project is to determine the extent to which ctDNA can inform on tumour heterogeneity in the patient. The success of objective 1 is crucial, as we continue to rely on ctDNA as a biomarker. An important aspect of this chapter will be utilization of multiple target mutations, testing ctDNA to assess the tumour composition of a patient. Currently, tumour heterogeneity is characterized through deep analysis of tumour samples, however, leveraging ctDNA to inform on this may provide a non-invasive and cost-effective alternative or adjunct method. The results from this objective are discussed in Chapter 3.

In several patients, I aim to determine if ctDNA from liquid biopsies can provide an accurate representation of the mutations observed in tumour. I will perform similar sequence analysis experiments on plasma and tumour and compare the mutations detected in both. I will determine the utility of ctDNA towards inference of the clonal structure of clones and sub-clones within a tumour. Tumour heterogeneity is known to change temporally, especially during the course of treatment. I aim to demonstrate this through ctDNA analysis of multiple plasma samples taken sequentially. The success of this may alleviate clinical reliance on tumour samples to monitor changes to tumour heterogeneity during treatment. Our experiments rely on tumour sample to inform on

suitable mutations to test in ctDNA. However, in cases with no available tumour samples, a strategy to identify suitable target mutations is needed. A method to discover variants using only ctDNA from a plasma sample may provide a solution. These "novel" variants can be used to continue monitoring ctDNA levels, assuming plasma samples are still obtained from the patient. I aim to assess the utility of ProDuSe, a python based toolkit capable of processing sequence reads from our experiments, to discover novel variants in ctDNA. As tumour heterogeneity can rapidly change in a patient during the course of treatment, there is a need for a robust method to inform on targetable somatic mutations without reliance on tumour biopsies.

1.7. Authorship Contributions

This project was conceived of primarily by Dr. Ryan Morin. I was responsible for performing all sample preparations, experimental techniques, DNA sequencing, and analysis of the findings. Patient samples and clinical data were provided by our collaborators Dr. Nathalie Johnson, Dr. Koren Mann and Dr. Sarit Assouline from Jewish General Hospital, and by our collaborators Dr. Joseph Connors and Dr. Randy Gascoyne from the BC Cancer Agency.

I wrote chapters 1 and 4 in their entirety. In chapter 2 and 3, targeted amplicon sequencing and hybridization capture experiments were conceived by Dr. Ryan Morin. I performed DNA extraction on all plasma samples, processed samples of whole blood to obtain plasma in certain patients, designed primers for amplicon sequencing, and performed all amplicon sequencing and hybridization capture experiments including product validation by gel electrophoresis or Qubit. Whole exome sequencing on tumour and normal samples were typically performed by our collaborators, and bioinformatics analysis to select for target mutations was done by Dr. Ryan Morin and myself. In various patients, I performed whole exome sequencing on tumour samples (extracted DNA from tumour biopsies or CTCs).

Development of hybridization capture methods including designing custom adapters and lockdown probes, testing and modifying library preparation protocols, analyzing hybridization efficiency and molecular barcode utility and function were done by Dr. Miguel Alcaide and me. I was primarily responsible for DNA sequencing of final amplicons and capture libraries, although for various experiments, DNA sequencing was

performed by Daniel Fornika or Kevin Bushell for convenience. I performed alignment of sequence reads, sequence analysis, and statistical testing of results and generated all the figures and tables in the results section. Figure 2.1 was taken from our modified library preparation protocol written by Dr. Miguel Alcaide and me.

ProDuSe software was designed and tested by Marco Albuquerque and Dr. Ryan Morin. Updates and fixes for ProDuSe was done by Christopher Rushton and Dr. Ryan Morin. I performed ProDuSe analysis on all hybridization capture experiments. Materials and Methods Sections 2.3.3 and 2.3.4 are partially based on a published manuscript (Assouline *et al*, 2016) of which I am a co-second author. I wrote all other sections in chapter 2 and 3.

Chapter 2.   Circulating   Tumour   DNA   as   a Biomarker

2.1. Abstract

Diffuse large B-cell lymphoma (DLBCL) patients are typically given conventional treatment, namely R-CHOP, upon diagnosis. Liquid biopsies may provide an effective means to monitor patients post-treatment. To test this, I applied two methods for detecting ctDNA: targeted amplicon sequencing and hybridization capture. In this chapter, I test 22 relapsed DLBCL patients for ctDNA at two time points: at the start of their clinical trial, and 15 days later. I successfully detected ctDNA in 20 of the 22 patients, with two patients having undetectable levels with either method. We found the hybridization capture method to be superior in terms of cost-effectiveness to targeted amplicon sequencing. Hybridization capture had the ability to multiplex significantly more mutations and was not limited by the presence of high molecular weight DNA in the samples. We found significant increases in ctDNA were correlated with a lack of response to treatment in 9 out of 13 non-responders with detectable ctDNA. Importantly, every responder tested was not associated with a significant increase in ctDNA. We conclude that a patient responding to treatment does not associate with a significant increase in ctDNA (Specificity = 100%).

2.2. Introduction

We sought to evaluate the level of ctDNA in a small cohort of 22 relapsed DLBCL patients (hereafter referred to as the QCROC cohort) and infer any potential relevance in the context of other available clinical data. These patients had all been diagnosed with either *de novo* DLBCL or tFL and had been relapsed or refractory following treatment with R-CHOP (rituximab, cyclophosphamide, doxorubicin, vincristine, and prednisone). This group of patients entered into a clinical trial evaluating the HDACi, Panobinostat, as a therapeutic for relapsed/refractory DLBCL (rrDLBCL). Exome sequencing on tumour and normal samples, taken at the start of the trial, had previously been done and these data allowed us to readily identify somatic mutations that could be utilized to specifically detect ctDNA in plasma. To quantify ctDNA, one or more target mutations was selected

from each patient and, where possible, we chose a variant in a gene known to be frequently mutated in lymphoma and having a high variant allele fraction (VAF) in the tumour. The VAF is the proportion of DNA molecules (or more typically, the unique sequence reads) representing a specific mutant allele at a locus relative to all DNA molecules at that locus.

Within the clinical trial, response to therapy was assessed in these patients by CT scan approximately 1 to 6 months, depending on patient or evaluated clinically. Using these data, we divided the patients into two categories: those whose tumour masses stayed similar or started to shrink in size (decrease in SPD) thus responding to treatment (responders), and those whose tumour masses continued to increase in size (increase in SPD) and thus did not respond to treatment (non-responders). Of note, these patients had continued treatment cycles and CT scans following this initial scan, so initial response may not be an accurate indication of a patient's overall outcome. We obtained plasma samples from these patients from two time points: plasma day 0 was taken at the start of Panobinostat treatment, and plasma day 15 was taken 15 days after the start of treatment. We chose to compare the change in ctDNA levels to the results from the initial scan because it was the nearest to the plasma samples available post-treatment, although the initial CT scans were performed at least 15 days after the second plasma sample was collected (i.e. one month after start of treatment). In any case, the patients deemed non-responders by this method at least showed no measurable response to their initial treatment. As such, these data would allow us to determine if ctDNA quantification in these patients could be a biomarker for treatment response.

In this chapter, I utilized two main experimental techniques to quantify ctDNA at specific loci: targeted amplicon sequencing and hybridization capture. I began by performing targeted amplicon sequencing as a preliminary test to determine if ctDNA was detectable in these patients. This method had several limitations that hamper its sensitivity including PCR and sequencing errors. The detection limit of ctDNA by NGS deep sequencing of amplicons is reportedly 0.01 to 2%[116], a rather broad range that is likely closer to 1% based on our experience. For analysis, we set a threshold at which ctDNA is considered undetectable by amplicon sequencing of 1% (VAF = 0.01), based on our experience with data from more sensitive techniques and excluded any counts below this value when using this method

To determine changes in ctDNA levels over time, I compared the VAF from day 0, effectively a baseline, to the day 15 plasma sample. Here, we used the VAF as a proxy for unique template molecules because individual template molecules cannot be readily discriminated without the use of molecular barcoding. To calculate the VAF from amplicon sequence data, I determined the ratio of the total number of mutant reads by the total reads spanning the target mutation regardless of the base represented at that site (i.e. all reads). To reduce the contribution of sequencing error, the base at a target mutation was required to agree on both the forward and reverse reads to be counted towards the total number, otherwise the read pair was discarded. This was deemed to provide a more robust and accurate determination of VAF. For various reasons, to be covered later in this and the following chapter, the VAF of a single mutation may not represent the level of ctDNA accurately but was nonetheless used for that purpose in this section.

For a subset of the patients tested, we were unsure if ctDNA was absent or below the sensitivity of the amplicon sequencing assay. We implemented a method involving hybridization capture as an alternative strategy to sequence ctDNA. Hybridization capture involves using a set of biotinylated probes to capture DNA fragments with regions of interest from cfDNA libraries. The probes used herein targets up to 53 known lymphoma-associated genes, which provides a relatively quick, cost-effective assay to quantify ctDNA at multiple positions

To enhance sensitivity and specificity, our protocol employed a modified library preparation using custom adapters with a molecular barcode of five degenerate bases. This allows suppression of PCR and sequencing errors present in a minority of duplicated DNA fragments. The custom adapter includes a three bp fixed tag, which is non-degenerate and complementary between positive and negative strands, that stabilizes the double strand adapter to improve ligation to DNA fragments. Errors from PCR or sequencing can be identified and removed, by "collapsing" DNA reads with unique barcodes. The collapsed reads (which represents the initial cfDNA molecules) are used to calculate the VAF for these experiments (detailed in Section 2.3.5).

2.3. Materials and Methods

2.3.1. DNA Extraction

Patient samples and data were obtained from collaborators at the Jewish General Hospital (JGH) in Montreal, Quebec. We were provided with DNA from a "normal" sample, typically taken from peripheral blood, and DNA from tumour samples obtained at day 0 and day 15. We were provided with matching plasma samples at day 0 and day 15 separated from blood, a small aliquot of 1 mL, which I used for DNA extraction. Blood samples collected at the JGH site were treated with Heparin, which acts as an anti-coagulant. These samples were collected before the availability of Streck BCT® (or a similar blood collection tube), which were developed to obtain high quality cell-free DNA with minimal contamination.

I extracted cfDNA from thawed plasma samples using the QIAamp® Purification of Circulating Nucleic Acids from Serum or Plasma kit (Qiagen), which uses a silica membrane to bind nucleic acids from the sample. I performed the extraction on all available plasma, which ranged from 0.5 to 2 mL starting volume per patient. PBS (phosphate buffered saline) was added to samples with less than 2 mL, to maximize efficiency. I modified this protocol by incubating the mixture of lysed plasma sample and binding buffer at room temperature, instead of on ice as described. I also added a third, pre-elution wash step. These modifications were done to decrease the concentration of salt in the eluted product, which contributed to a lower PCR yield. I eluted the product in the provided elution buffer (Buffer AVE) in an initial volume of 50 µL (elution 1). I performed a second "elution 2" step in a volume of 200 µL to maximize the yield of extracted DNA from the silica membrane and to serve as an emergency back-up. In all cases, elution 1 provided enough DNA to perform the experiments described in this chapter, thus elution 2 was not required. Elutions 1 and 2 were stored at -20°.

2.3.2. Targeted amplicon sequencing

I designed all primers semi-manually using Primer3 (http://bioinfo.ut.ee/primer3/) and the UCSC genome browser in-silico PCR. These primers are capable of amplifying the region surrounding the target mutation, and are referred to as site-specific primers. I attempted to limit the length of the amplified PCR product to 150 bp and placed the

target mutation site in the middle to allow high-quality sequence coverage in both directions. In certain cases, high GC content inhibited successful primer design. I overcame this by designing longer fragments (200 to 250 bp). Site-specific primers had a universal sequence added to the 5' end (Universal sequence for forward: 5'-CGCTCTTCCGATCTCTGNNNN-3' and reverse: 5'-TGCTCTTCCGATCTGACNNNN-3') which allow a second, nested PCR using Illumina P5/P7 primers. Site-specific primers were ordered (IDT) in 100 µM aliquots.

For the first round of the nested PCR (PCR1), I added at least 10 ng of input DNA. This PCR reaction includes Q5 polymerase and the site-specific primers in a 50 µl reaction volume for 30 cycles (98°C 30 s, 30 cycles of 98°C 10 s, 57°C 30 s, 72°C 7 s, 1 cycle of 72°C 2 min). The PCR1 products were purified with 1.8x volume of AMPure XP (Agencourt) according to the Manufacturer's protocol to remove excess primers and validated by agarose gel electrophoresis and Qubit fluorometric quantitation (Thermo Fisher Scientific). PCR1 products act as templates for the second round of nested PCR (PCR2). PCR2 primers (Illumina P5/P7) anneal to the universal sequences on the PCR1 products, and contain the full-length Illumina adapter sequences allowing cluster generation and sequencing and also include a 6 nt index for sample identification during the demultiplexing stage. The nested PCR2 was done using Q5 polymerase in a 50 µl reaction volume for 6 cycles (98°C 30 s, 6 cycles of 98°C 10 s, 65°C 30 s, 72°C 30 s, 1 cycle of 72°C 5 min). PCR2 products were purified and validated as described for PCR1.

All products from targeted amplicon sequencing experiments were sequenced by Illumina MiSeq according to the manufacturer's protocol. I used MiSeq Reagent Kit V2 with a read length of 2 x 150 bp. Products from one sample were given at least 10% of a sequence run (2.5 million reads). FASTQ files generated by the MiSeq, which contain raw sequence data and quality scores, were used to align to a human reference genome (hg18 was used for these experiments) using BWA (http://bio-bwa.sourceforge.net/) and aligned sequences were visualized in IGV (http://software.broadinstitute.org/software/igv/). Base calls at the target mutation that agreed on both strands were totalled to determine VAF using a custom python script.

2.3.3. Library preparation for tumour and plasma samples

Recent advances to library construction methods have enabled routine construction of Illumina sequencing libraries from small amounts of fragmented DNA. Concurrent with this work, various groups demonstrated the successful construction of libraries from cell-free DNA (cfDNA) from cancer patients[117,118,119]. We adopted a strategy similar to that used by Newman *et al*[117] with custom modifications enabling error suppression in DNA sequencing and the recognition of DNA damage and PCR-induced artifacts. Briefly, the "duplex sequencing" strategy involves the incorporation of custom double-stranded adapters constructed with a semi-degenerate region for molecular barcoding[114]. In our variation of duplex sequencing, we implemented a semi-degenerate region in each adapter oligonucleotide to act as a molecular barcode while facilitating hybridization of the semi-complementary molecule. The adapters are ordered as single-stranded DNA oligonucleotides (IDT) and are hybridized in equimolar concentration to generate functional Y-shaped double-stranded adapters. This design includes a short stretch (three bp) of non-degenerate nucleotides that are complementary between strands, which act to stabilize the adapters to improve ligation efficiency with a DNA molecule (Figure 2.1).

Extracted DNA from plasma samples were used to prepare libraries for hybridization capture experiments. I used an input range of 10 to 15 ng, as DNA was limiting, using the KAPA Low Throughput library preparation kit for Illumina platforms (Roche). This library preparation method involves an "end-repair" reaction followed by an "A-tailing" reaction in the presence of AMPure XP magnetic beads (Agencourt) according to the manufacturer's protocol. Subsequently, I perform a ligation in the presence of a 30-fold molar excess of our custom Y-shaped adapters for libraries prepared from plasma. Our custom adapters were composed of the annealing of the two following DNA oligonucleotides: 5'-ACACTCTTTCCCTACACGACGCTCTTCCGATCT**WSWSW**GAC*T-3' and 5'-/5Phos/GTC**WSWSW**AGATCGGAAGAGCACACGTCTGAACTCCAGTC-3'. Our custom adapters contained a five bp degenerate barcode (bolded bases shown in the DNA oligonucleotides). This provides a potential of 1,024 barcode permutations ($2^{(5+5)}$) (Figure 2.1). Our custom adapter and molecular barcode allowed for error suppression from PCR and sequencing errors.

I purified the ligated products with two rounds of 0.8x volumes of AMPure XP (Agencourt) to remove excess and self-ligated adapters generated during ligation. I amplified libraries with six bp indexed primers using 6-9 cycles of PCR, depending on the input mass of DNA. Following this, I performed a final round of purification with 0.8x volume of AMPure XP and total library yields were measured using Qubit fluorometric quantitation (Thermo Fisher Scientific). Successful libraries were inspected for fragment size distribution using a Bioanalyzer 2100 (Agilent), a highly sensitive method for performing gel electrophoresis. A successful library would have a low peak at 150 bp and a high, sharp peak at 300-400 which contains the library (Figure 2.2A). A problematic library can be identified by a sharp peak at 150 bp, which represents the self-dimerization of adapters due to a lack of cfDNA for successful amplification (Figure 2.2B). In this example, the peak at 300 bp representing the library is still present, but at a lower ratio. In this scenario, the sample would typically have a lower than expected sequence depth (after combining reads from the same initial ligation) due to reduced library complexity.
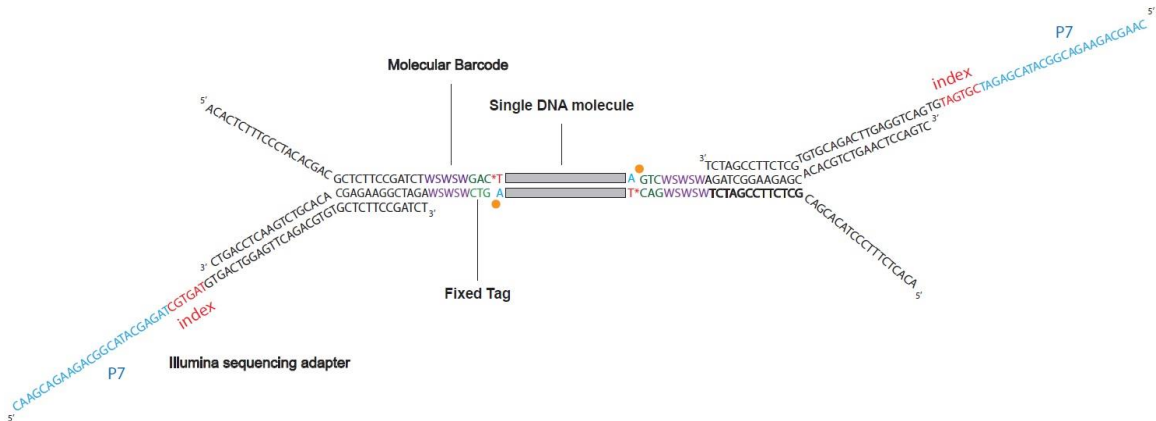
Figure 2.1.   Diagram of molecular barcode and fixed tag
The Y-shaped custom adapter is ligated onto a DNA molecule (gray block) and contains the molecular barcode (purple) and a fixed tag (green) at the 3' end. Index (red): Six bp index used for sample identification during demultiplexing. P7 (blue): Illumina adapter used for sequencing.
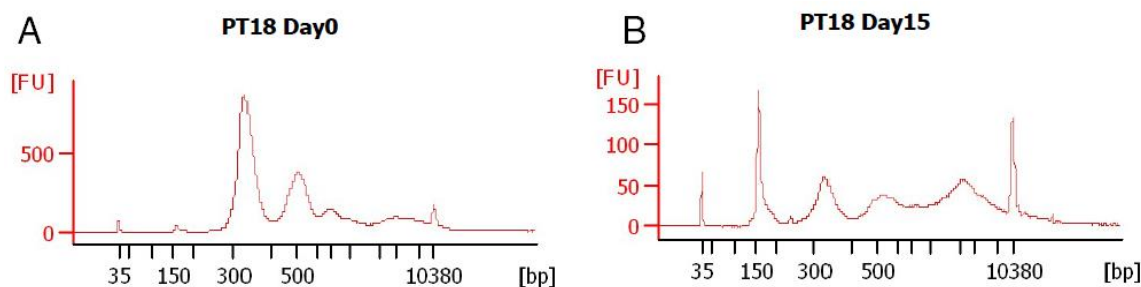
Figure 2.2.   Comparison between successful and problematic library preparation
Electropherogram of two samples post-library preparation. Y axis: FU – Fluorescent units, X axis: bp – base pair length (A) Patient 18 day 0 sample shows successful library preparation with a peak at the correct base pair length (300 to 400 bp). (B) Patient 15 day 15 sample shows a problematic library with a sharp peak at 150 bp and a relatively lower peak at the expected 300 to 400 bp length.

2.3.4. Hybridization capture

We employed hybridization capture with a pool of custom probes to perform ctDNA detection and quantification. The prepared DNA libraries are pooled together in equimolar concentration, between 4 to 10 libraries (samples) per capture. 5 µg Human Cot-1 DNA® (Thermo Fisher Scientific) and 3 nmol of a custom xGen® Blocking oligonucleotide (IDT) were added to the mixture, and completely dried out in a vacuum concentrator. I re-suspended the dried pellet with 8.5 µl of 2x Nimblegen SeqCap EZ® Hybridization buffer (Roche), 3.4 µl Nimblegen SeqCap EZ® Hybridization enhancer (Roche), and 1.1 µl of ultra-pure water. Re-suspension was done by agitation at room temperature for 10 min, followed by denaturation of the pool at 95°C for 10 min. I added 3-4 pmol of a pool of xGen Lockdown® probes (IDT) and the library/probe mixture was incubated at 65°C for a minimum of 4 hours.

The xGen Lockdown® probes targeted the exons and hotspots of a panel of lymphoma-associated genes. The process involved the design of a panel of biotinylated 120-nt single-stranded DNA "lockdown" oligonucleotides (IDT) that tile across regions of interest (typically exons). xGen Lockdown® oligonucelotides were chosen over competing methodologies from Agilent or Roche Nimblegen because they could be ordered in 96-well plates to generate many variations of pooled probes. This flexibility allowed us to capture and sequence specific sets of genes, or can be used to assemble a restricted set of probes to deeply target a set of loci (typically important hot spots).

I used three different gene pools, as we continued to design probes throughout this project. The first panel included exons and hotspots for *FOXO1*, *MS4A1*, *PIM1*, *BCL2*, *CD58*, *MYC*, *NFKBIE*, *MYD88*, *CCND3*, *EZH2*, *CD79B*, *BCL2*, *MEF2B*, *FAS*, *STAT6*, *HIST1H1E*, *B2M* and *SOCS1* (hereafter referred to as the "IDT173x pool"). The second panel included exons and hotspots for *EZH2*, *CREBBP*, *MLL2*, *STAT6*, *FAS*, *MEF2B*, *TP53* and *EP300* (hereafter referred to as the "IDT HME pool"). Our extended lymphoma panel (hereafter referred to as "IDT EXLYM pool") included exons and hotspots for *STAT6*, *MYD88*, *CD79B*, *CCND3*, *EZH2*, *BCL2*, *MEF2B*, *TP53*, *ID3*, *TCF3*, *FAS*, *B2M*, *HIST1H1E*, *SOCS1*, *FOXO1*, *MS4A1*, *CD58*, *NFKBIE*, *MYC*, *PIM1*, *TNFAIP3*, *TNFRSF14*, *MLL2*, *ETS1*, *TMEM30A*, *IL4R*, *CARD11*, *TBL1XR1*, *TMSB4X*, *CREBBP*, *GNAI2*, *HIST1H1C*, *SGK1*, *NOTCH1*, *P2RY8*, *GNA13*, *IRF8*, *BTG2*, *EBF1*, *KLHL6*, *CCND1*, *BCL10*, *EP300*, *ZFP36L1*, *PTPN1.* The IDT173x pool was designed for preliminary testing of hybridization capture experiments, and was relatively limited in size compared to the other two pools. The IDT HME and IDT EXLYM pool comprehensively cover all the genes, and were the main pools used in these experiments.

Hybridized DNA/probe fragments were captured with 50 µl of Streptavidin M-270 Dynabeads™ (Thermo Fisher Scientific) at 65°C for 45 min. Hybridized libraries were subsequently washed with 100 µl pre-warmed Wash Buffer I (65°C), two washes with 200 µl pre-warmed Stringent Wash Buffer (65°C) and final washes with Wash Buffers I, II and III, sequentially, at room temperature. All wash buffers were supplied by the Nimblegen SeqCap® EZ capture kit (Roche). The hybridized DNA and Streptavidin beads were amplified by PCR using Illumina P5/P7 primers and the KAPA HiFi DNA polymerase mastermix in a reaction volume of 50 µl for 12 cycles (98°C 45 s, 12 cycles of 98°C 15 s, 60°C 30 s, 72°C 30 s, 1 cycle of 72°C 1 min). Final products were sequenced by Illumina MiSeq according to the manufacturer's protocol. I used MiSeq Reagent Kit V2 with a read length of 2 x 150 bp. Each library (sample) within the final product was given at least 10% of a sequence run (2.5 million reads).

2.3.5. ProDuSe

In order to analyze raw sequence data generated from our modified library construction method, another student in our lab developed ProDuSe (processing duplex sequencing), a python based toolkit designed to handle sequence reads with molecular barcodes thereby leveraging this information to suppress errors in the data. ProDuSe

takes sequence reads from a FASTQ file (generated by the Illumina MiSeq) as input and identifies both the fixed tag and degenerate molecular barcode, trims these from the sequence and retains this information in the read name. Any reads with a molecular barcode having more than N mismatches, where N is an established value depending on length of barcode, are excluded by the software to prevent two distinct molecules sharing the same sequence by chance. For these experiments below, wherever ProDuSe was used, I consistently used a value of N=3.

After trimming, ProDuSe aligns the resulting reads using BWA-MEM (http://bio-bwa.sourceforge.net/). For experiments using ProDuSe, I consistently used the hg19 reference genome (GRCh37). After alignment, reads sharing the same mapping coordinates are assigned to an adapter family based on having a similar barcode sequence, and all reads within an adapter family are collapsed into a consensus sequence. Collapsing takes into consideration the most common base at each position across all reads in a family, essentially removing minority bases (i.e. the collapsed read contain the most frequent bases observed). With sufficient coverage, errors from PCR or sequencing are thereby removed if they are represented by the minority bases. The software tracks the number of individual reads that contribute to each consensus family such that subsequent analyses can differentiate these from lower-quality consensus sequences. The resulting collapsed FASTQ files are finally realigned with BWA-MEM and the bam file is directly interpreted in IGV. I use the bam file containing the collapsed read families for determining VAF of target mutations. Notably, this software is still in active development and my work used a combination of ProDuSe and manual review of aligned reads (in IGV) to calculate VAF. The latest version of ProDuSe is available at https://github.com/morinlab/ProDuSe/tree/master/ProDuSe.

For results generated from ProDuSe collapsed reads, I calculated VAF using individual molecule counts. Collapsed reads represent one strand from the initial DNA molecule present during library preparation. ProDuSe provides a tally of each base within a collapsed read. For these experiments, the VAF was calculated as the proportion of collapsed mutant bases relative to all bases reported at a specific locus (i.e. the target mutation).

2.3.6. Statistics

Standard error for each VAF was determined by a 95% confidence interval (CI) as shown in the equation below:

$$95\% \, CI = 1.96 * \sqrt{\frac{1}{cov} * \frac{mut}{cov} * \frac{ref}{cov}}$$

where cov = total reads, mut = mutant reads, ref = reference reads

In this study, line graphs showing VAF change from day 0 to day 15 have the error bars included for quick comparison to see if they overlap. In general, if the error bars do not overlap, we can conclude the VAF change is significant. However, overlapping error bars do not necessarily mean the VAF change is insignificant. Rather, no conclusion can be drawn about significance.

For targeted amplicon sequencing, coverage (total reads) was very high at the target mutation, so error bar overlap was not expected. For hybridization capture, the collapsed total reads were much lower in comparison, so the 95% CI was much higher. To determine true significance, I used the Fisher's exact statistical test. My test utilized the number of mutant reads and reference reads at the target position for day 0 and day 15, however this depended on the experiment. For targeted amplicon sequencing, the number of mutant and reference reads referred to the number of sequence reads that aligned to our reference genome. For hybridization capture, the number of mutant and reference reads referred to the number of individual molecules determined by unique consensus sequences. The one-tailed hypothesis is the proportion of mutant reads that change in one direction (increase or decrease) from day 0 to day 15, with the null hypothesis that there is no significant change.

To perform the Fisher's exact test, we need to tabulate our mutant and reference reads through a contingency table (Table 2.1). The p-value for the one-tailed Fisher's exact test was generated in R, using the equation below:

$$p = \frac{(a+b)! * (c+d)! * (a+c)! * (b+d)!}{a! * b! * c! * d! * n!}$$

where n = a + b + c + d

Due to the capabilities of the program, the lowest, possible p-value was 2.2 x 10^-16. For this study, a p-value equal to or below this number is considered zero.

Table 2.1. **Contingency table used for determining significance of change in VAF**

	Number of mutant reads	Number of reference reads
Day 0	a	c
Day 15	b	d

2.4. Results

2.4.1. Targeted amplicon sequencing on QCROC cohort

I performed targeted amplicon sequencing on 22 patients from the QCROC cohort, testing two plasma samples (day 0 and day 15) per patient. I detected ctDNA in at least one plasma sample for 16 of the 22 patients (Figure 2.3 and Figure 2.4). Detected ctDNA was determined by a calculated VAF greater than 0.01 at the target mutation. The remaining 6 patients with undetectable ctDNA were not included in statistical analysis.

Eight patients were classified clinically as responders (Figure 2.3A and Figure 2.3B). Patients (or PT) 12, 18 and 32 showed high VAFs at day 0 at the target mutation that decreased considerably down to a negligible value. Patients 4, 13 and 15 at day 0 had detectable, but relatively low VAFs between 0.01 and 0.04. These patients still showed a decrease in VAF at day 15. Patient 4 and 15 had almost overlapping trends in VAF change, however this was simply a coincidence. The remaining two patients, PT17 and PT35 had VAFs at their respective target mutations below 0.01 for both time points, so were considered to have undetectable ctDNA. Thus, six of the eight responders had detectable ctDNA. In all responding patients, changes in VAF was determined to be statistically significant by a one-tailed Fisher's exact test, except in cases where VAF was below 0.01 and the statistical test was not performed.

We were able to confidently detect ctDNA in samples from 10 of 14 non-responders in total. In six of these, namely patients 3, 22, 26, 30, 40 and 39, the level of ctDNA had increased significantly in the subsequent time point (Figure 2.4A and Figure 2.4B). This increase in VAF was determined to be statistically significant by a one-tailed

Fisher's exact test. Interestingly, I found two of the non-responders, patients 11 and 25, to have a significant change in ctDNA levels that was discordant from their clinical response (Figure 2.4C). This discordance could potentially be resolved by analyzing more mutations within these patients.

In the remaining non-responders, namely patients 5, 7, 19, 20, 33 and 36, we had limited sensitivity for ctDNA (Figure 2.4D). All but two samples had undetectable ctDNA (VAF < 0.01). These two samples were plasma samples at day 15 from PT05 and PT19, considered detectable because of a reported VAF greater than 0.01 (0.0110 and 0.0103, respectively), which allowed us to include these two patients in the analysis. Assuming a ctDNA level of zero (undetectable) at day 0, the increase in VAF to a detectable level was determined to be statistically significant by a one-tailed Fisher's exact test. Lastly, patients 7, 20, 33 and 36, had undetectable ctDNA at both time points (VAF < 0.01).

In extracting cfDNA, the yield of DNA can sometimes inform on the presence and amount of ctDNA in a sample, but there are a number of factors that are known to confound this. Among these samples, extracted DNA from elution 1 showed a broad range of yield spanning 1.5 ng/μl to almost 25 ng/μl in one patient (PT18 day 15), with a mean yield of 5 ng/μl. Specifically, elution 1 was performed using a 50 μl volume, resulting in a total yield of DNA across patients from approximately 70 ng to 1240 ng, with a mean yield of 264.36 ng (Table 2.2). Samples with total yields less than 2 ng/μl (100 ng yield) were relatively low compared to expected yields (mean yield) from plasma extractions. Unsurprisingly, patients 17 (day 0 only), 20, 33, 35 and 36 (day 15) all had less than 100 ng extracted DNA from elution 1. These five are among the six patients with undetectable ctDNA in this study. The remaining sixth patient (PT07) had yields greater than 100 ng (Day 0: 612 ng, Day 15: 148 ng). Interestingly, PT30 day 15 was the only sample with less than 100 ng yield (76 ng), but was shown to have detectable ctDNA.

In cases with relatively high yields compared to the mean yield, there was concern that normal cells in the blood had lysed before DNA extraction could take place, contributing to an increase in total DNA. For example, PT18 showed a steep decrease in ctDNA at day 15 (Figure 2.3B), which could be attributed to wild-type DNA from normal cells. The presence of un-fragmented DNA released into plasma by lysis of nucleated

blood cells (i.e. non-cfDNA) in a sample is referred to as high molecular weight (HMW) DNA contamination. The difference in yields from day 0 to day 15 in this patient was substantial: 209.5 to 1240 ng (Table 2.2). Additionally, the electropherogram of PT18 day 15 library (Figure 2.2B) suggests there is much less cfDNA, despite the higher yield.

I performed gel electrophoresis experiments to test for high molecular weight DNA contamination in the remaining samples using the highly sensitive Bioanalyzer 2100 (Agilent) to separate DNA libraries by size. For example, PT05 day 0 showed several broad peaks from ~800 bp and longer, representing the HMW DNA contamination from normal cells in the blood (Figure 2.5A). This is contrasted in PT04 day 0, a good example of pure ctDNA, where those broad peaks are missing, and there is only the presence of a peak at 300 bp representing the ctDNA (Figure 2.5B). Unsurprisingly, PT05 day 0 had undetectable ctDNA with a VAF of 0.0051 (Table 2.2). HMW DNA contamination may convolute our reported VAF estimates by heavily skewing the amount of wild-type (normal) base calls in a sample, thus it is important to remove this from our experiments. We used a unique approach involving AMPure XP (Agencourt) magnetic beads to size select for DNA fragments in the range of 150 to 180 bp (referred to as "reverse-AMPure"). Although reverse-AMPure was successful at removing the HMW DNA contamination, the overall DNA yield from this approach was unfortunately much lower than desired (Figure 2.5C).
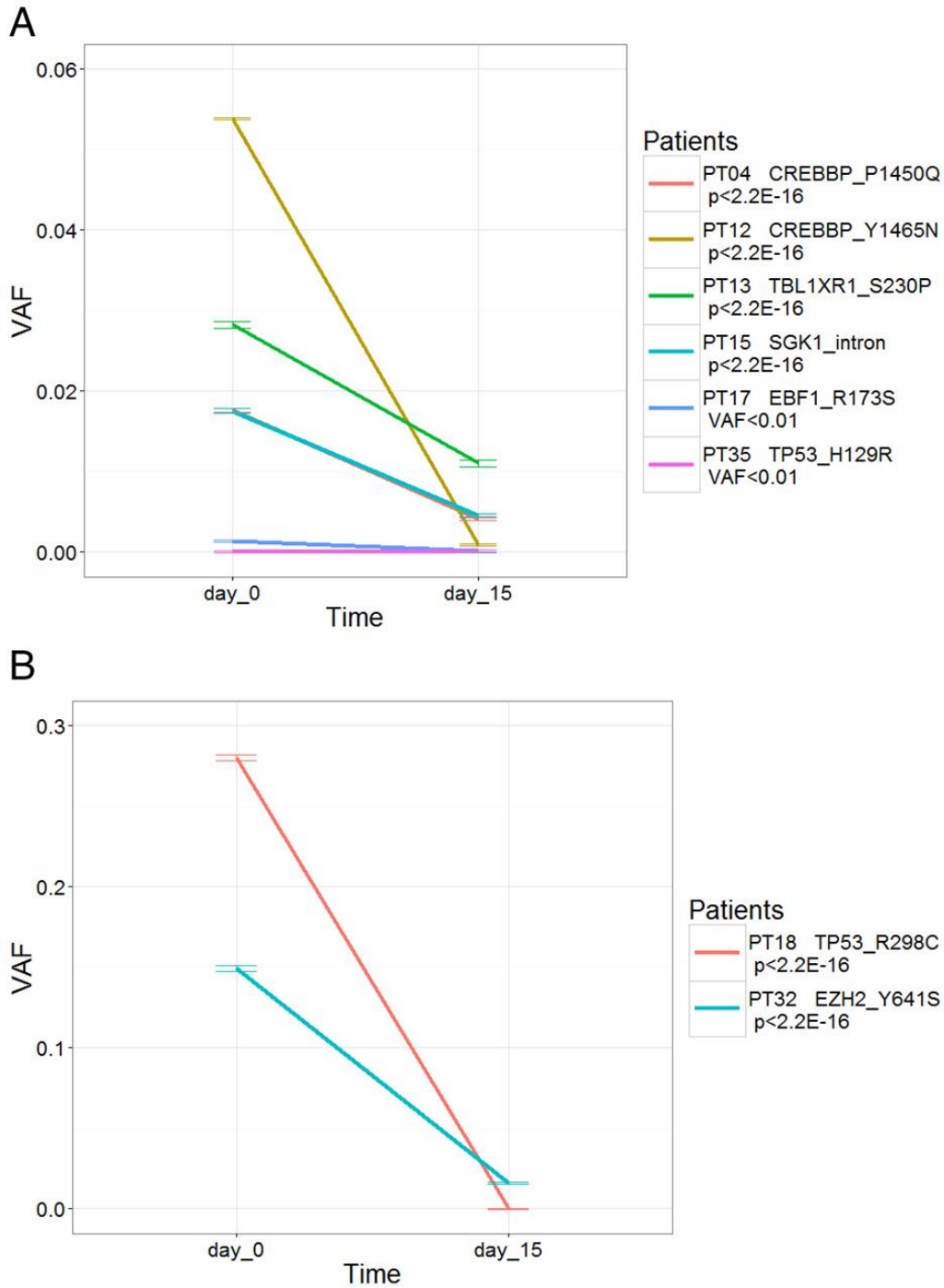
Figure 2.3.   Targeted amplicon sequencing results for responders
Line graph shows VAF change of QCROC patients responding to treatment from day 0 to day 15 with 95% confidence intervals included as error bars. Target mutation is shown next to patient ID (including gene name and amino acid change) with p-value from one-tailed Fisher's exact test below (unless VAF<0.01). (A) Four patients with significant decreases in VAF, where VAF for all samples were reported below 0.06, and two patients (PT17 and PT35) determined to have undetectable ctDNA with VAF less than 0.01. (B) Two patients with at least one sample showing a high VAF above 0.1. Both patients had a significant decrease in VAF.

33
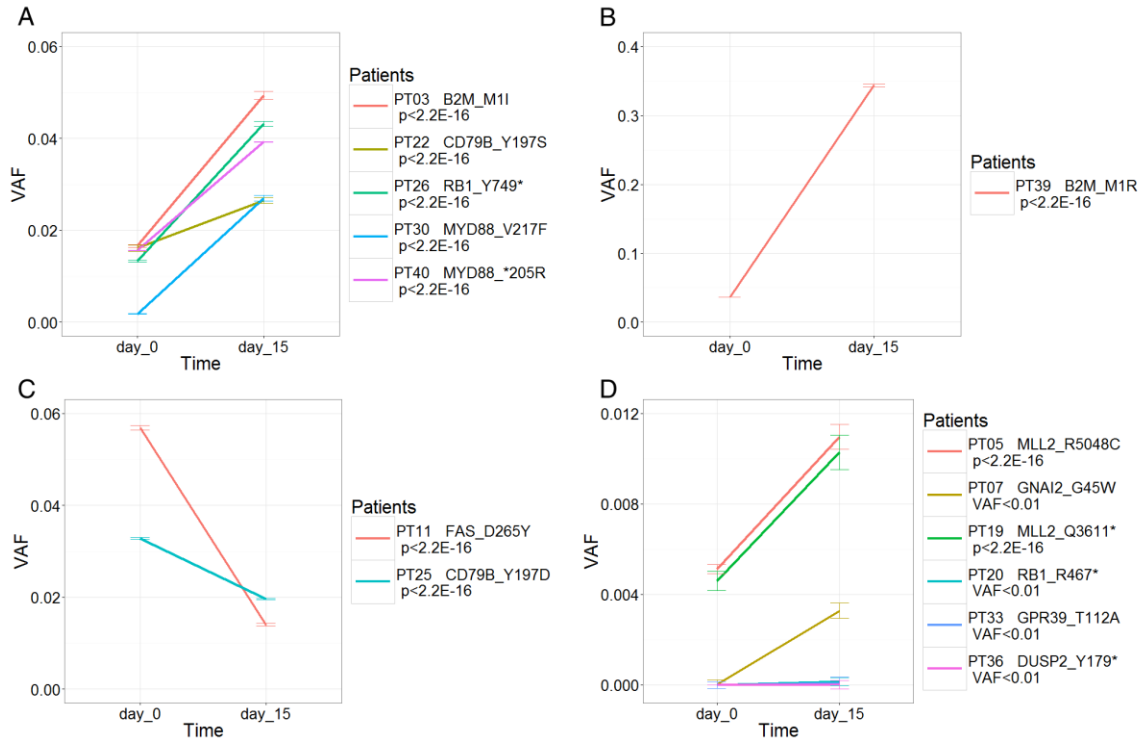
Figure 2.4.   Targeted amplicon sequencing results for non-responders
Line graph shows VAF change of QCROC patients not responding to treatment from day 0 to day 15 with 95% confidence intervals included as error bars. Target mutation is shown next to patient ID (including gene name and amino acid change) with p-value from one-tailed Fisher's exact test below (unless VAF<0.01). (A) Five patients with VAF below 0.06, where at least one time point had VAF above 0.01. These patients showed a significant increase in VAF. (B) Patient 39 had the highest reported VAF of 0.35 at day 15, compared to all samples. (C) Two non-responding patients showing a significant discordant decrease in VAF. (D) Six patients with reported VAF in all samples below 0.012. Four patients are considered to have undetectable ctDNA (VAF < 0.01). The remaining two patients had undetectable ctDNA at day 0 but reported VAF above 0.01 by day 15.

Table 2.2. Yield, VAF and coverage from QCROC experiments

Sample	Total DNA extracted from elution 1 (ng)	Amplicon Sequencing		Hybridization Capture	
		VAF	Total reads	Mean VAF	Mean collapsed reads
PT03 Day 0	175.5	0.0166	939440	0.3301	85.8
PT03 Day 15	246	0.0494	221328	0.4431	288.5
PT04 Day 0	133	0.0175	1357315	0.1406	106.7
PT04 Day 15	299	0.0042	371698	0.0375	133.3
PT05 Day 0	338.5	0.0051	666680	0.0000	9.0
PT05 Day 15	219	0.0110	176153	0.1811	63.5
PT07 Day 0	612	0.0000	490617	0.1258	201.3
PT07 Day 15	148	0.0033	174577	0.1163	332.3
PT11 Day 0	290.5	0.0569	816176	0.2337	223.7
PT11 Day 15	367	0.0140	493841	0.1762	193.0
PT12 Day 0	183.5	0.0538	347127	0.4117	266.0
PT12 Day 15	301	0.0009	292000	0.0056	534.0
PT13 Day 0	361	0.0282	557659	0.1300	311.5
PT13 Day 15	317.5	0.0110	191876	0.1012	257.0
PT15 Day 0	317	0.0175	788599	0.0677	197.0
PT15 Day 15	317.5	0.0045	402941	0.0274	194.7
PT17 Day 0	76.5	0.0013	1145616	0.0249	294.3
PT17 Day 15	296.5	0.0001	425078	0.0000	453.0
PT18 Day 0	209.5	0.2802	267025	0.3657	216.0
PT18 Day 15	1240	0.0000	87225	0.0000	138.0
PT19 Day 0	129	0.0046	105629	0.0065	463.5
PT19 Day 15	269	0.0103	72813	0.0563	106.5
PT20 Day 0	82	0.0000	1226056	0.0000	1081.0
PT20 Day 15	97	0.0001	487724	0.0142	353.0
PT22 Day 0	105	0.0161	325573	0.0302	488.5
PT22 Day 15	531	0.0265	252382	0.1304	253.0
PT25 Day 0	157	0.0328	258270	0.2236	178.2
PT25 Day 15	134.5	0.0196	382240	0.0548	243.3
PT26 Day 0	143.5	0.0133	1550489	0.0294	475.7
PT26 Day 15	152	0.0432	462332	0.0988	718.3
PT30 Day 0	1046	0.0018	1130349	0.0000	431.0
PT30 Day 15	76	0.0270	307268	0.1111	81.0
PT32 Day 0	412.5	0.1491	139995	0.2974	723.0
PT32 Day 15	287	0.0137	164090	0.1407	200.8
PT33 Day 0	73	0.0000	607673	0.0437	343.5
PT33 Day 15	28	0.0001	220704	0.0880	221.5
PT35 Day 0	68.5	0.0000	913136	0.0000	636.3
PT35 Day 15	97.5	0.0001	285355	0.0000	238.7

Sample	Total DNA extracted from elution 1 (ng)	Amplicon Sequencing		Hybridization Capture	
		VAF	Total reads	Mean VAF	Mean collapsed reads
PT36 Day 0	210.5	0.0000	307117	0.0000	n/a
PT36 Day 15	92	0.0000	124392	0.0000	n/a
PT39 Day 0	249	0.0365	1225274	0.2532	186.4
PT39 Day 15	340.5	0.3438	224423	0.3004	275.3
PT40 Day 0	165	0.0156	545028	0.2650	100.0
PT40 Day 15	238	0.0393	450436	0.3226	700.5
Responders Average	307.34	0.0364	483545.9	0.1094	306.27
Non-responders Average	239.80	0.0281	508749.4	0.1298	311.44
Total Average	264.36	0.0311	499584.5	0.1224	309.47
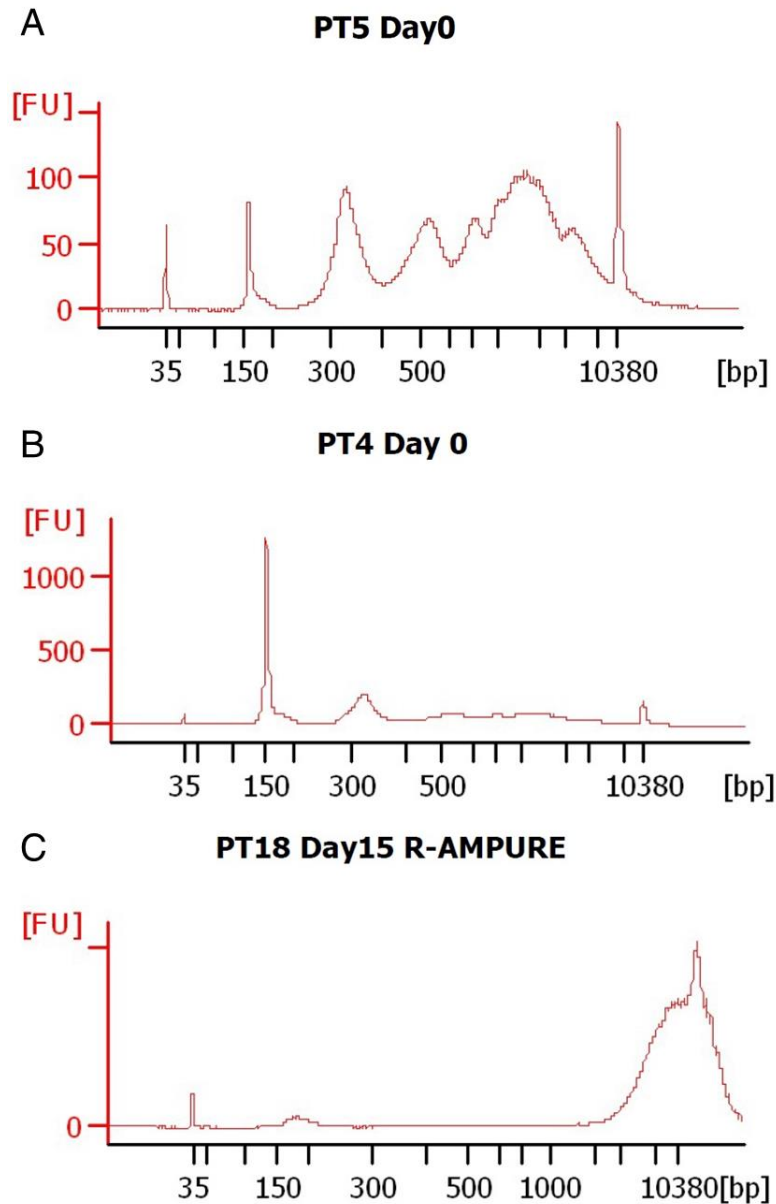
Figure 2.5.   Electropherogram of DNA samples using the Agilent Bioanalyzer 2100

The amount of DNA is measured in fluorescent units (FU) on the y axis, and the size of fragments is measured in base pairs (bp) on the x axis. (A) cfDNA from patient 5 day 0 plasma, a patient suspected to have high molecular weight contamination. Several broad peaks observed from 800 bp and larger represent the high molecular weight DNA component. (B) cfDNA from patient 4 day 0 plasma, an example of almost pure ctDNA, characterized by a broad peak at 300 bp. (C) Resultant DNA fragments from patient 18 day 15 plasma with high molecular weight DNA contamination removed by "reverse-AMPure".

2.4.2. Analysis of QCROC samples using hybridization capture with molecular barcoding

Successful removal of HMW DNA contamination from our samples with reverse AMPure was not consistent. We decided on another strategy capable of capturing small fragments while excluding large fragments. Using hybridization capture, we were able to prepare libraries from only cfDNA. With this method, HMW DNA fragments were too large for successful library amplification, while small cfDNA fragments were ideal. This allowed us to sequence ctDNA from the QCROC cohort, unimpeded by HMW DNA contamination.

Hybridization capture is able to target hundreds of target positions, allowing us to analyze multiple mutations for each patient. This is important for patients with changes in VAF discordant from clinical results. I used the IDT173x pool on a small subset of patients for preliminary testing, and once the IDT HME and IDT EXLYM pools were designed, switched to using those pools for the remaining patients and initial subset of patients to ensure consistency across the cohort. Hybridization capture was more sensitive than amplicon sequencing, able to detect ctDNA in more patients. Of the 22 QCROC patients, I detected ctDNA in 20 patients, with a mean VAF (the average VAF of all target mutations within one patient) greater than 0.01 in at least one time point (Figure 2.6 to Figure 2.11). This is an 18% increase from amplicon sequencing, where only 16 of 22 patients had detectable ctDNA. The two remaining patients (PT35 and PT36) remain undetectable through hybridization capture (and were undetectable by amplicon sequencing). There was no hybridization capture data to present for these two patients (VAF = 0 for both time points).

I successfully detected ctDNA in seven of eight responders (Figure 2.6 and Figure 2.7). All seven patients showed a concordant decrease in mean VAF that was determined to be statistically significant by a one-tailed Fisher's exact test. PT18 and PT12 showed a steep decrease in mean VAF, where all target mutations showed a similar trend of decreasing VAF (Figure 2.6A and Figure 2.6B). PT17 (patient with undetectable ctDNA from amplicon sequencing), had a low mean VAF of 0.025 at day 0, which decreased to 0 at day 15 (Figure 2.6A). Although the confidence intervals at day 0 were quite broad due to low VAFs, *MEF2B* had a higher reported VAF (0.04) than *EBF1* (0.012), which was the single target mutation for amplicon sequencing of this patient

(Figure 2.6C). This highlights the importance of using multiple target mutations to improve sensitivity for detecting ctDNA. Read support in PT17 day 15 was sufficient (453 mean collapsed reads), and was higher than day 0 (294 mean collapsed reads), which supports the reported VAF of 0 at day 15 (Table 2.2)

PT04 and PT32 showed significant decrease in mean VAF (Figure 2.7). Individual target mutations for these patients all showed similar decreasing change in VAF (Figure 2.7B and Figure 2.7C). PT15 was the only responder with an individual target mutation (*MLL2* +AA insertion) that showed minor change in VAF with overlapping confidence intervals, which was inconsistent with the mean VAF. However, this patient had another target mutation in *MLL2* (+C insertion) affecting a different exon and a target mutation in *EZH2* that both showed a decrease in VAF consistent with our expectations (Figure 2.7D). All but two responders (PT13, Figure 2.6A and PT15, Figure 2.7A) had non-overlapping confidence intervals when comparing mean VAFs.

I detected ctDNA in 13 of 14 non-responders (Figure 2.8 to Figure 2.11). Patients 5 and 30 were non-responders that showed a significant increase in mean VAF (Figure 2.8A). Read support was low in both these patients, with a mean of 64 collapsed reads in PT05 day 15 and a mean of 81 collapsed reads in PT30 day 15, which resulted in relatively large 95% CIs (Table 2.2). However, a complete lack of ctDNA at day 0 results in the reported increase at day 15 to be considered significant. The individual target mutations (*MLL2* and *BCL2)* of PT05 are completely zero at day 0, and show similar increasing trends in VAF contributing to a significant result (Figure 2.8B). It should be noted that the read support for PT05 day 0 is very low (9 mean collapsed reads), and may not be sufficient to accurately determine VAF at this time point. PT20 is another patient with a relatively large 95% CI at day 15, however in this case it is due to a low VAF at day 15 (VAF = 0.014) (Figure 2.9A), as read support was above the average (Table 2.2). Similar to the previous patients, an absence of ctDNA at day 0 resulted in this patient showing a significant increase in VAF at the target mutation.

In four of the non-responders with detectable ctDNA, namely PT22, PT26, PT19 and PT33, I observed typical increases in mean VAF that were determined to be significant. PT22, PT26 and PT19 were cases where each individual target mutation showed consistent trends in VAF change (Figure 2.8C, Figure 2.9B and Figure 2.9C) compared to the trend in mean VAF change (Figure 2.8A and Figure 2.9A). We do not

always observe consistent trends across all target mutations, as shown in PT33, where we observed an inconsistent minor change in VAF of the *TMSB4X* mutation. The other target mutation, a silent mutation in *NOTCH1*, showed a comparatively distinct increase in VAF, which provided support for an overall increase in mean VAF in this patient (Figure 2.9D).

Patient 7 and 40 were the only two non-responders that did not attain significance (Figure 2.10A and Figure 2.11A). Interestingly, PT07 showed a slight decrease in mean VAF. There were six target mutations detected in this patient with no striking trend in VAF change (Figure 2.10B). Non-responders PT39 and PT3 were also cases where I detected ctDNA in six or more target mutations, although in these cases the mean VAF across these mutations showed a significant increase (Figure 2.10A and Figure 2.11A). Interestingly, PT39 showed at least two different mutations with different trends in VAF change in *FAS, MS4A1* and *NFKBIE*. Strikingly, the different mutations affecting the same gene show inconsistent changes in VAF with each other. For example, we observe the K287E missense mutation in *FAS* (dark green) and the E257* nonsense mutation in *NFKBIE* (dark purple) to consistently increase in VAF, whereas the L18* nonsense mutation in *FAS* (gray) and the frameshift insertion (+TC) in *NFKBIE* (brown) remain relatively unchanged (Figure 2.10C). PT03 showed consistent increases in VAF for the individual target mutations *B2M* (blue), *CD58* (purple), and *GNAI3* (pink) (Figure 2.11B).

Lastly, patients 11 and 25 were non-responders with a significant decrease in mean VAF, which is discordant from what we expect (Figure 2.10A and Figure 2.11A). PT11 had multiple mutations showing decrease in VAF, with mutations such as *TMSB4X* (brown) and *MYC* (yellow) showing significant decrease in VAF where 95% CI for these values do not overlap (Figure 2.10D). PT25, initially shown as discordant with PT11 from targeted amplicon sequencing, still remains significant for a decrease in VAF, supported by all individual target mutations (Figure 2.11C).
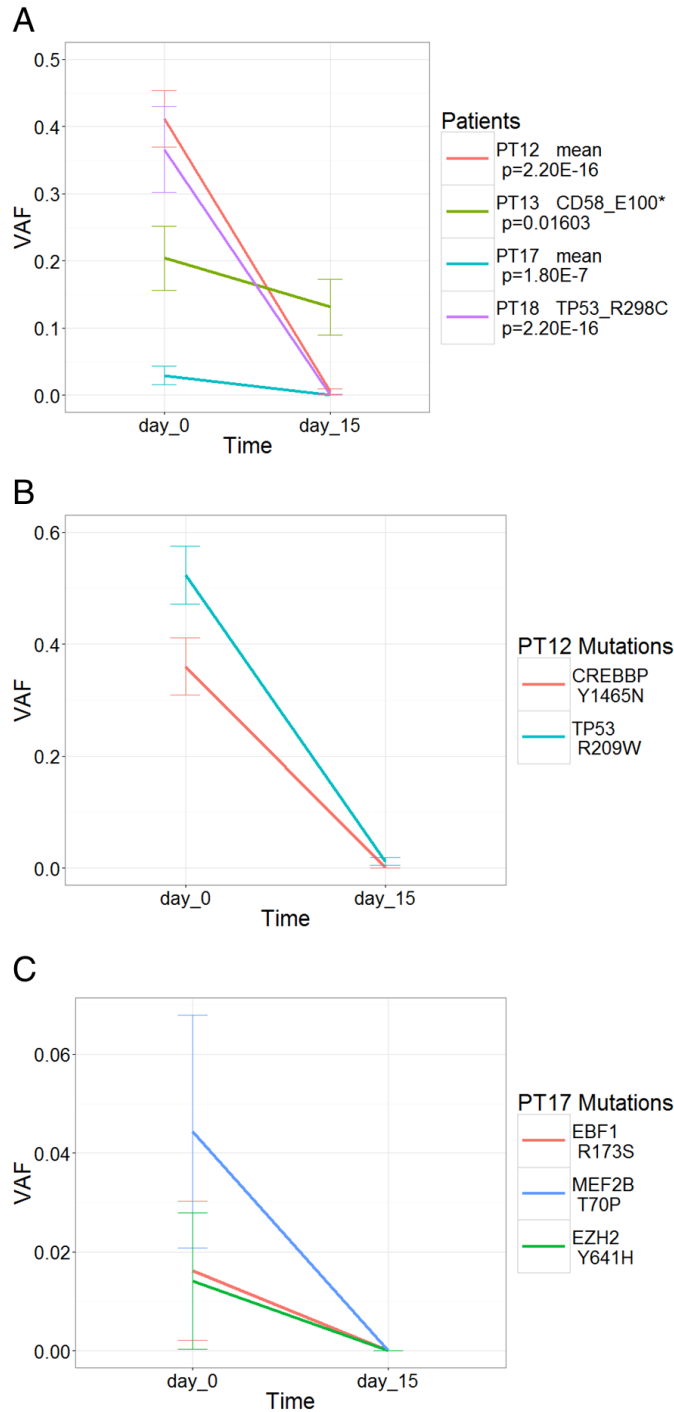
Figure 2.6.   Hybridization capture results for responders
Line graph shows changes in VAF from day 0 to day 15 at target mutations (including gene name and amino acid change) for QCROC patients responding to treatment. 95% confidence intervals are included as error bars for each VAF. (A) Two responders (detailed in B and C) showing significant decreases in mean VAF across target mutations, and two responders showing significant decreases in VAF at a single target mutation. P-values from one-tailed Fisher's exact test are shown below patient ID. (B) Analysis of PT12 using two target mutations, where consistent decreases in VAF are observed. (C) Analysis of PT17 using three target mutations, where all three mutations was deemed absent at day 15, based on a VAF of 0.

41
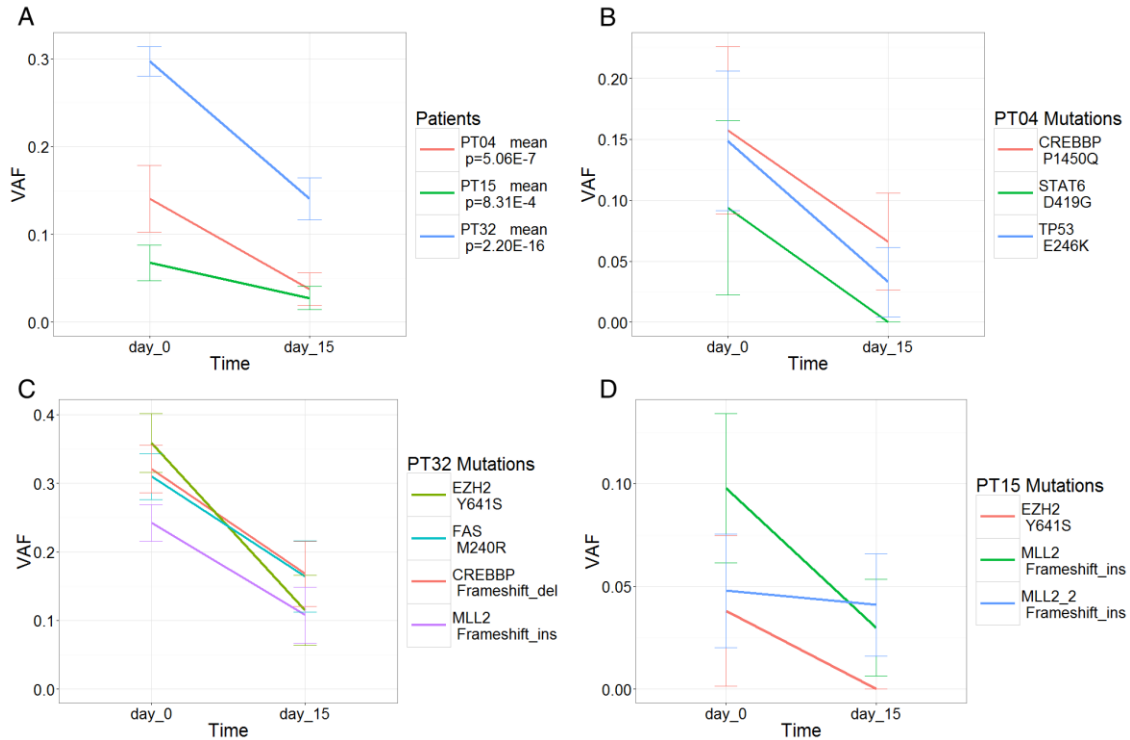
Figure 2.7.   Additional hybridization capture results for responders
Line graph showing changes in VAF from day 0 to day 15 at target mutations (including gene name and amino acid change) of QCROC patients responding to treatment. 95% confidence intervals are included as error bars for each VAF. (A) Three responders (detailed in B, C and D) showing significant decreases in mean VAF across target mutations. P-values from one-tailed Fisher's exact test are shown below patient ID. (B) Analysis of PT04 using three target mutations, where we observe consistent changes in VAF. (C) Analysis of PT32 using four target mutations. Three mutations show consistent trends, while the *EZH2* mutation (green) showed a sharper decrease in VAF. (D) Analysis of PT15 using three target mutations. An *MLL2* insertion (+C, green) affecting exon 36 decreased significantly below the VAF level of another *MLL2* insertion (+AA, blue) affecting exon 39, which maintained a consistent VAF between day 0 and day 15. The *EZH2* mutation was deemed to be absent at day 15, based on a VAF of zero.

Figure 2.8.   Hybridization capture results for non-responders
Line graph showing changes in VAF from day 0 to day 15 at target mutations (including gene name and amino acid change) of QCROC patients not responding to treatment. 95% confidence intervals are included as error bars for each VAF. (A) Two non-responders (detailed in B and C) showing significant increases in mean VAF across target mutations, and one non-responder (PT30) showing significant increases in VAF at a single target mutation. P-values from one-tailed Fisher's exact test are shown below patient ID. (B) Analysis of PT05 using two target mutations, where the change in VAF is almost identical. (C) Analysis of PT22 using four target mutations with consistent trends in VAF change.
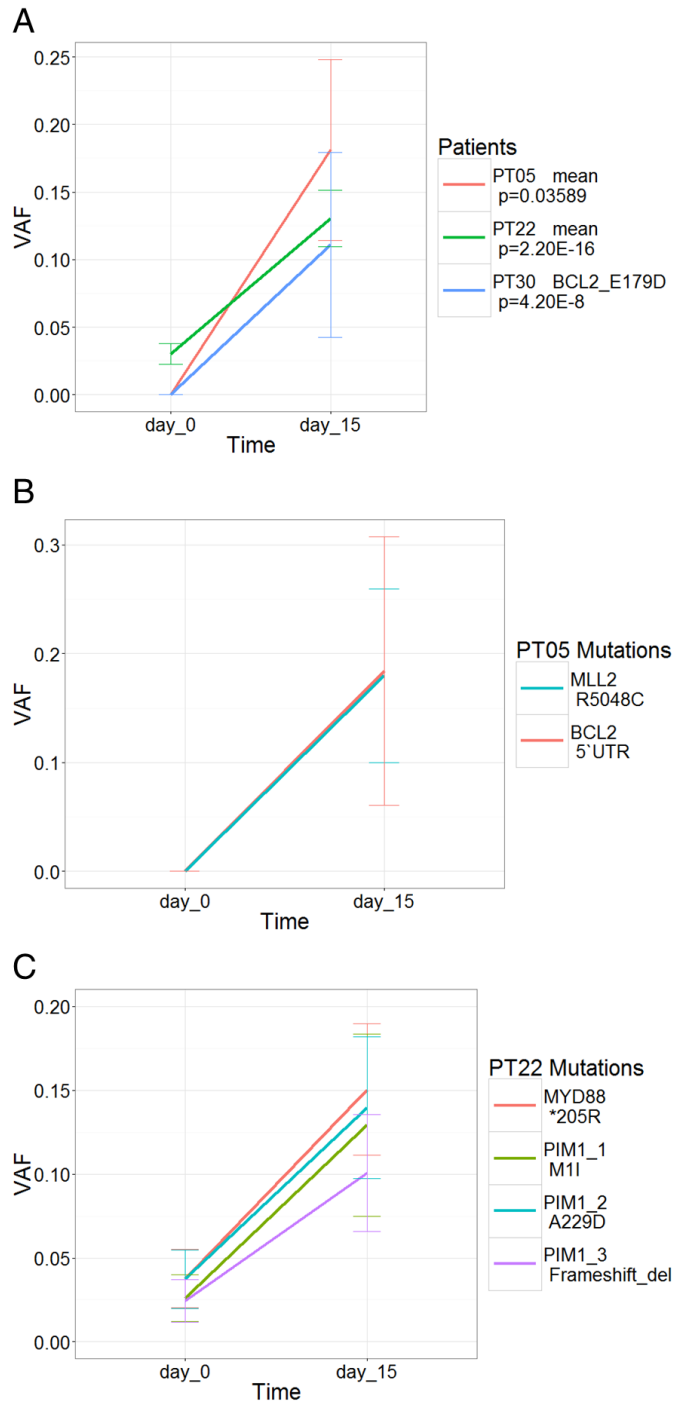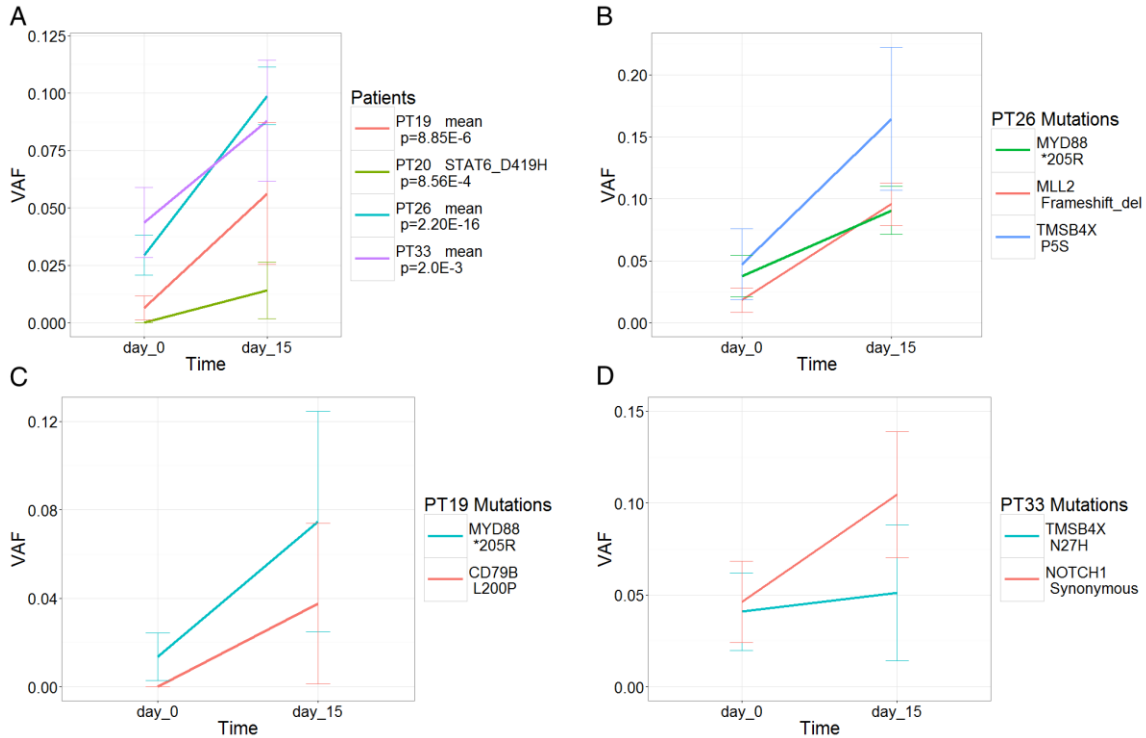
Figure 2.9.   Hybridization capture results for non-responders with low VAF

Line graph showing changes in VAF from day 0 to day 15 at target mutations (including gene name and amino acid change) of QCROC patients not responding to treatment. 95% confidence intervals are included as error bars for each VAF. (A) Three non-responders (detailed in B, C and D) showing significant increases in mean VAF across target mutations, and one non-responder (PT20) showing significant increases in VAF at a single target mutation. P-values from one-tailed Fisher's exact test are shown below patient ID. (B) Analysis of PT26 using three target mutations, with all mutations showing a consistent increase in VAF. (C) Analysis of PT19 using two target mutations, with consistent trends in VAF change. (D) Analysis of PT33 across two target mutations. The VAF for a silent mutation in exon 34 of *NOTCH1* showed a steeper increase than the VAF for a missense mutation in *TMSB4X*.

44

Figure 2.10. Hybridization capture results for non-responders with six or more target mutations

Line graph showing changes in VAF from day 0 to day 15 at target mutations (including gene name and amino acid change) of QCROC patients not responding to treatment. 95% confidence intervals are included as error bars for each VAF. (A) Three non-responders (detailed in B, C and D), where all but PT07 showed a significant change (decrease for PT11, increase for PT39) in mean VAF across target mutations. P-values from one-tailed Fisher's exact test are shown below patient ID. (B) Analysis of PT07 across six target mutations, showing assorted trends in VAF change. (C) Analysis of PT39 across ten target mutations, six of these occurred in three genes, *FAS*, *MS4A1* and *NFKBIE* (two target mutations each). (D) Analysis of PT11 across seven target mutations, showing assorted trends in VAF change.
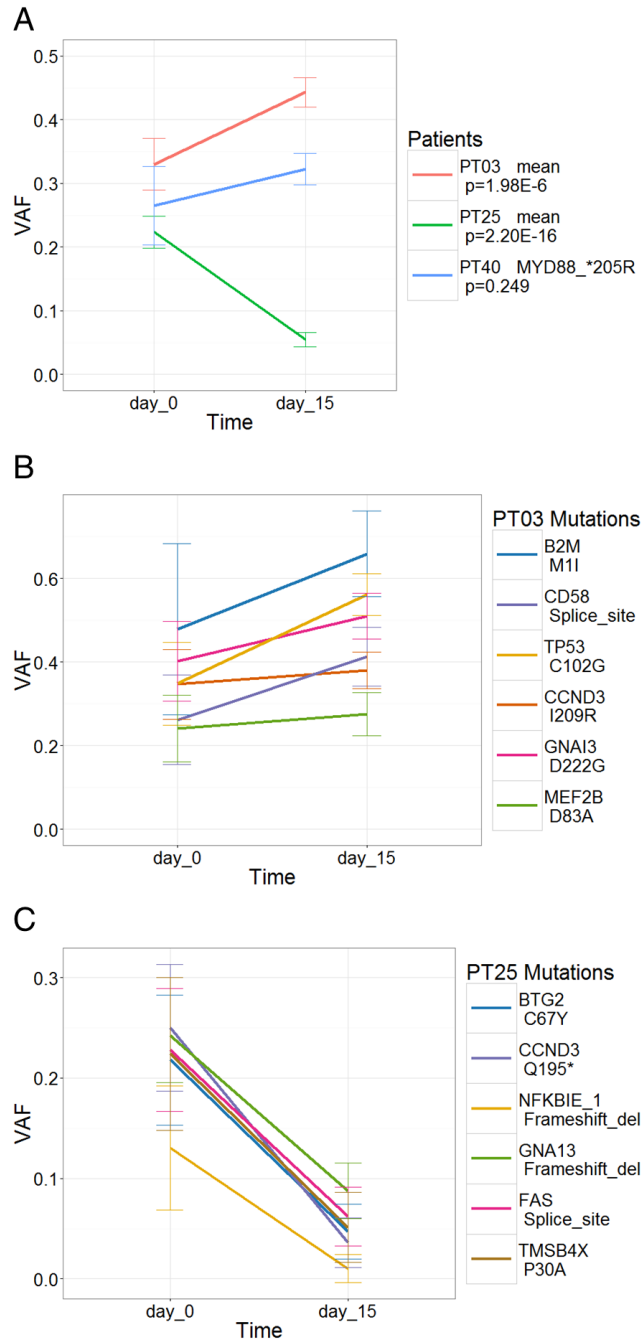
Figure 2.11.   Hybridization capture results for non-responders (with a discordant case)
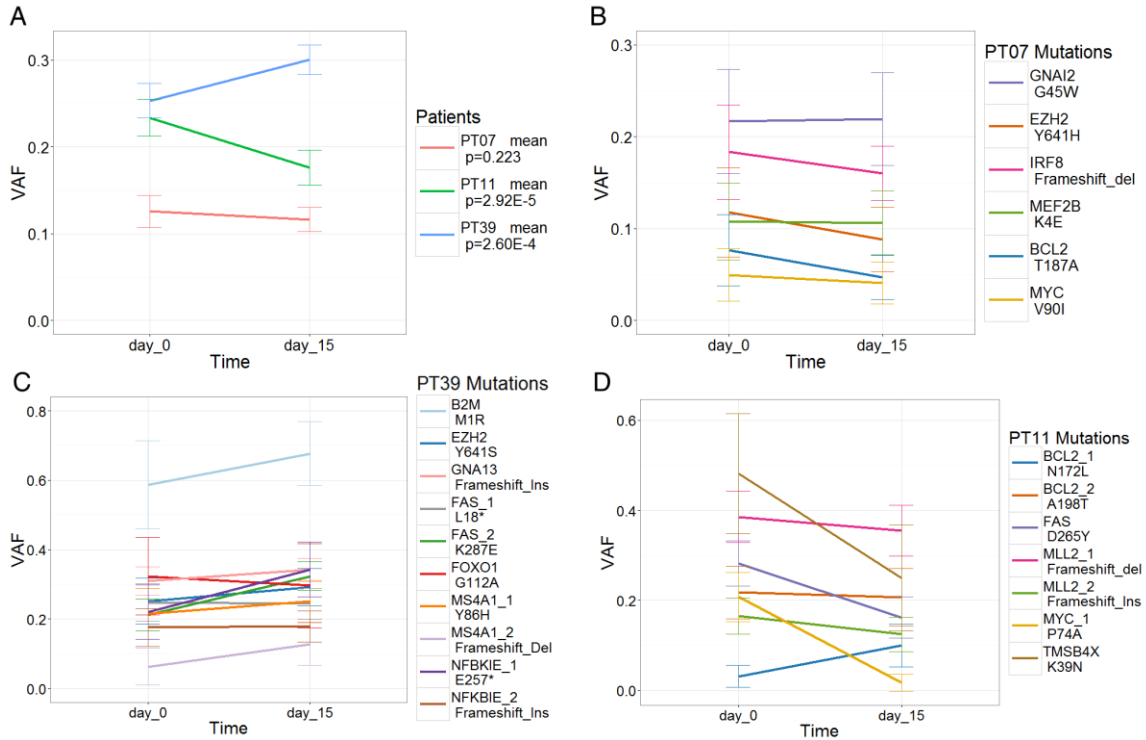
Line graph showing changes in VAF from day 0 to day 15 at target mutations (including gene name and amino acid change) of QCROC patients not responding to treatment. 95% confidence intervals are included as error bars for each VAF. (A) Two non-responders (detailed in B and C) showing a significant change (increase for PT03, decrease for PT25) in mean VAF across target mutations, and one non-responder (PT40) showing a statistically insignificant increase in VAF at a single target mutation. P-values from one-tailed Fisher's exact test are shown below patient ID. (B) Analysis of PT03 using six target mutations, where we observe consistent increases in VAF change in at least three mutations (*B2M, CD58, GNAI3*). (C) Analysis of PT25 using six target mutations, where all mutations showed a consistent trend in decreasing VAF.

2.5. Discussion

The targeted amplicon sequencing experiments I applied to plasma samples from the QCROC cohort were useful as a preliminary screen for evidence of ctDNA and its potential suitability as a biomarker. I confirmed the presence of ctDNA in 16 of 22 patients (73%) using a conservative minimum threshold of a VAF greater than 0.01. Undetected ctDNA in six patients cannot be readily explained by insufficient coverage at the target mutation, three of these patients having an average (between day 0 and day 15) coverage exceeding the total average across all patients (Table 2.2). Lowering the VAF threshold may reduce the number of patients with undetectable ctDNA however a suitable threshold would need to be determined. For example, PT07 day 15 had a VAF of 0.003, which was considered to be undetectable. However, if we used the lowest threshold reported in the literature (0.001)[116], PT07 day 15 would be among the patients with detected ctDNA. Although reporting more patients with detectable ctDNA may benefit the results of this study, I found a threshold VAF of 0.001 was too low and not justified given the error profile of the data. Extensive testing within our methods could help optimize this threshold.

Target mutations were chosen from previous WGS/WES results from tumour and must be associated with lymphoma. I selected mutations affecting the exons of these lymphoma-associated genes in all but one patient for amplicon sequencing. In this case (PT15, Figure 2.3A), I used a target mutation within the intron of *SGK1*. Although mutations affecting the exons are preferred, I did not choose such target mutations for this patient. Exonic mutations can affect protein sequences unlike intronic ones, however intronic mutations are still useful as a biomarker as long as they are somatic. The objective was to track and quantify ctDNA, which is ambivalent to the functional effect of the mutation.

In my results, I represent the estimate of standard error for the calculated VAFs with a 95% confidence interval (CI). On average, the CI for the amplicon sequencing results were much smaller than for hybridization capture (shown as error bars for each VAF). To generate the CI, I used the total number of reads and number of mutant reads (detailed in Section 2.3.6). In general, the larger the total number of reads, the smaller the CI. Thus, samples with deeper coverage at the target mutations would have smaller CIs which would less likely overlap. This is evident from amplicon sequencing, where the

average coverage was much larger due to the nature of deep sequencing. The average coverage with amplicon sequencing in these experiments was approximately 500,000x, compared to 310 mean collapsed reads from hybridization capture. Unsurprisingly, the CIs for each VAF data point from hybridization capture experiments (Figure 2.6 to Figure 2.11) are much larger than for amplicon sequencing (Figure 2.3 and Figure 2.4). Despite very narrow CIs for amplicon data, I am wary that these are over-estimates of the accuracy because each read is not a true independent measurement. The reported p-values from targeted amplicon sequencing were also very small in the majority of cases ($p < 2.2 \times 10^{-16}$). The Fisher's exact test was performed on un-collapsed sequence data from one amplicon per patient. As such, the reported mutant and reference reads used in this calculation are comprised of many PCR duplicates, some originating from the same molecule. Because of this issue, the reported p-values are artificially smaller than the true level of confidence. This limitation is overcome by our molecular barcoding system used in the subsequent section.

The line graphs showing VAF changes from both experiments in these patients all include the CIs as a visual aid to quickly assess the significance of the change (Figure 2.3, Figure 2.4, and Figure 2.6 to Figure 2.11). CIs alone do not allow significant changes to be identified. Rather, they provide an estimated range of values which contain the true VAF. From our results, there were only three patients (PT13, PT07 and PT40) with hybridization capture results showing overlapping CI in mean VAF between time points. As expected, these were not significantly different but the broad CI also suggests we were under-powered to properly assess this. In PT07 and PT40, the change in VAF is small, leading to overlapping CI. As expected, the p-values from a one-tailed Fisher's exact test for these two patients are greater than 0.05 (p = 0.223 and 0.249, respectively), which confirms the change in VAF was not significant. In contrast, for PT13 (Figure 2.6A), coverage was sufficiently high and although the change was modest in magnitude, the decrease in VAF was still determined to be statistically significant (one-tailed Fisher's exact test).

The relatively low coverage from hybridization capture results and consequentially broad CIs was concerning. However, it is important to note that the total coverage used to calculate CIs was determined after collapsing raw reads with the same barcode and mapping coordinates into a consensus sequence. In many cases, the amount of collapsed reads was half the amount of raw sequence reads, greatly reducing

the total coverage while increasing the CI. Although this seems counter-intuitive, it is more informative to have the collapsed reads than a high number of raw reads for analysis. The collapsed reads reflect the individual molecules present in the sample whereas raw reads consist of many duplicates and contain erroneous bases. The duplicate rate of individual molecules would not necessarily be controlled or balanced due to sampling effect from sequencing. So the calculated VAF and CI determined from individual molecule counts are the most accurate measure of the sample. The PCR-based method does not allow molecules to be collapsed and this is a unique feature of capture-based methods and is further enhanced by the presence of our molecular barcodes. When reporting mean VAF and coverage for hybridization capture experiments, I reported mean coverage as the mean count of collapsed reads (Table 2.2). Collapsed reads are a more accurate measure of coverage compared to raw sequence reads, since the VAF is determined from collapsed reads. The mean collapsed reads is essentially the average number of individual molecules supporting a target mutation in a patient. This metric was useful in comparing relative support for variant calling in each sample.

An important benefit of collapsing raw sequence reads to a consensus sequence is the removal of erroneous bases. Erroneous bases that are observed in the minority of duplicates are "collapsed out" in the consensus sequence, where the most observed base is kept. In several of our cases, the mutant VAF of the collapsed reads was zero, compared to very low (but non-zero) VAFs from the raw reads. This is important when determining the significance of the VAF change in a patient. An increase in VAF from a very low mean VAF may not be considered significant if the second sample has a low mean VAF, or if overall coverage is relatively small. However, an increase in VAF from a zero mean VAF to a sufficiently large VAF typically showed significance. The calculated p-values from the Fisher's exact test using the collapsed reads from hybridization capture were generally higher than when using all aligned sequence reads from targeted amplicon sequencing, although in the majority of these cases, the change in VAF was still determined to be significant ($p < 0.05$). Only PT40 showed insignificant change ($p = 0.249$) with hybridization capture, compared to a significant change ($p < 2.2 \times 10^{-16}$) inferred from targeted amplicon sequencing. However, as discussed above, this difference is likely due to a lower than average number of collapsed reads at day 0 (100

mean individual molecules) and we cannot firmly conclude from this result whether the ctDNA level was different.

The cause of reported undetectable ctDNA in samples is uncertain. As explained earlier, a lack of coverage is an unlikely cause. A low yield of extracted DNA from plasma may suggest a low level of cfDNA and thus a low level of ctDNA. Strikingly, many patients with undetectable ctDNA from targeted amplicon sequencing had relatively low yields from DNA extractions, however, this does not explain cases such as PT07, which had undetectable ctDNA despite relatively high yields. Additionally, PT30 day 15 had a relatively low yield (76 ng) but nonetheless reported a VAF of 0.027. Notably, we were able to detect ctDNA in all but two of these patients (ctDNA remain undetectable in PT35 and PT36) using hybridization capture, which suggests targeted amplicon sequencing lacks the sensitivity required to detect ctDNA in these problematic cases. Reasonably, in cases with undetectable ctDNA such as PT35 and PT36, improving sensitivity may allow detection, either by deeper sequencing of these samples or by using a method with higher sensitivity.

One complication we encountered in our analysis of the QCROC cohort was the effect of HMW DNA contamination on each methodology. The contamination was likely from healthy white blood cells that lysed in the sample tube, resulting in an influx of large fragments of normal DNA. For PCR-based analyses, this effectively diluted the cfDNA templates and skewed our VAF measurements, causing an underestimate in our assessment of total ctDNA. HMW DNA is, by definition, less fragmented than cfDNA, which results in unhindered amplification of these larger fragments by PCR. Fragmentation of genomic DNA during apoptosis leads to an average fragment size equivalent to a mononucleosome[120] such that PCR cannot amplify from templates in scenarios where forward and reverse priming sites are far apart. In ctDNA that is not contaminated with HMW DNA, fragments from the tumour are equally likely to be suitable templates. However in samples contaminated with HMW DNA from lysed non-tumour (blood) cells, primers can successfully amplify from virtually all fragments, greatly increasing the chance of wild-type fragments being amplified.

I performed gel electrophoresis experiments to detect HMW DNA contamination in samples, using two simple approaches: agarose gel electrophoresis and using the Bioanalyzer 2100 (Agilent). Both approaches successfully showed the presence of large

DNA fragments, but are time consuming and expensive when used on a high number of samples. I helped design an experiment to test the presence of HMW DNA by quantitative PCR, which has the benefit of parallelizing samples and reporting quantitative measurements. We used a very large target (*TLR3*, expected size: 1600 bp) that would provide an estimate of large fragment DNA, and should not be detected in any samples with pure apoptotic cfDNA due to the shorter template length. However, this method was not successful in our QCROC samples, due to the presence of the anti-coagulant, Heparin, which inhibited our qPCR reactions. Therefore, it is important that Heparin is not used when collecting blood samples for ctDNA analysis. Specialized tubes capable of stabilizing white blood cells such as Streck tubes[121] should be used to prevent HMW DNA contamination. Notably, hybridization capture experiments circumvented the problem of HMW DNA contamination. We found that when using this method, fragments larger than the expected sizes of cfDNA are not efficiently included in the final library and are naturally excluded. The only problem these samples caused for hybridization capture, was the actual yield (sequence depth) from sequencing was lower than expected because a significant fraction of the DNA was not included in the library.

From amplicon sequencing of the non-responders, we found two patients (PT11 and PT25) showing a discordant decrease in VAF at the target mutation. The VAF of one mutation may not accurately reflect the level of ctDNA in a patient, so hybridization capture was used to assess multiple mutations to determine a mean VAF. However, these two discordant patients still showed a significant decrease in mean VAF, and therefore are likely to have decreasing levels of ctDNA. One possible explanation is that the patient may not have started relapsing until after the plasma sample was obtained. The CT scans used to determine treatment response were performed at least two weeks after the day 15 plasma was drawn, potentially providing time for sudden growth in tumour burden. This could also explain why we have 4 non-responding patients that did not show a significant increase in ctDNA.

Given the varied mechanisms by which panobinostat may induce response in DLBCL, we also examined early changes in ctDNA as a potential biomarker for relapse or progression. In contrast to the other biomarkers examined, ctDNA levels were strongly associated with changes of tumour burden. In all but two patients measured, ctDNA was detected in at least one plasma sample and in 90% of cases, we observed significant changes in ctDNA relative to the day 15 sample. For most patients, these

experiments were performed on DNA extracted from 1 mL of plasma and prospective collection of larger volumes for ctDNA analysis should yield superior sensitivity among patients with lower levels. Despite the small sample size, we observed striking trends towards changes in ctDNA after 15 days of therapy and a clear association with response, with very high specificity and positive predictive value (PPV). No patients with an increase in ctDNA at day 15 ultimately responded to treatment and all patients who eventually responded had a significant drop in ctDNA after 15 days of therapy. Overall survival and progression free survival were also each significantly associated with a decrease in ctDNA. Thus, ctDNA dynamics may provide an early indication of ultimate treatment failure in clinical trials and mutational analysis could serve as an adjunct to other methods to study disease response and tumour genetics.

2.6. Conclusions

With the enhanced sensitivity afforded by our hybridization capture method and with a larger set of mutations to analyze, I was able to detect ctDNA in at least one of the two plasma time points in 20 of 22 patients. Overall, 40 of 44 total samples had at least 0.01 VAF, with an observed maximum VAF of 0.554 in one sample (PT03). Mean VAF was 0.136 and median VAF was 0.097.

Hybridization capture was more efficient and less hampered by limitations that accompany targeted amplicon sequencing, especially in light of variable sample quality for the retrospective cases. Specifically, the effect of HMW DNA contamination was solved by utilizing hybridization capture in all patients. The ability to concomitantly measure mutations among many genes in one assay allowed for quicker, cost-effective, and detailed analyses.

Data from CT scans taken one to six months after relapse classified 14 patients were non-responders and eight patients were responding to the treatment. Of those 14 patients undergoing relapse, nine patients showed significant increase in ctDNA from day 0 to day 15 plasma, four patients did not show significant increase (including two patients that showed a significant decrease), and one did not have detectable levels of ctDNA. Conversely, all eight responders showed a significant decrease in ctDNA from day 0 to day 15 plasma.

Based on these data, if a significant increase in ctDNA at day 15 is considered as a predictor for lack of response (as compared to insignificant change or decrease), the sensitivity, specificity, PPV and negative predictive value (NPV) are 69.2%, 100%, 100% and 63.6%, respectively. Although not all patients with decreased ctDNA eventually showed a sustained response, when comparing to the best response, the sensitivity and NPV remained at 100%. Hence, by measuring changes in ctDNA, these data show that patients unlikely to benefit from the therapy may be readily recognized early in the treatment course.

Chapter 3. Characterizing Tumour Heterogeneity with ctDNA

3.1. Abstract

Non-Hodgkin lymphoma are known to exhibit intra-tumour, temporal and spatial heterogeneity[122]. Monitoring changes in clonal structure in a NHL tumour over time requires a method capable of detecting genetic alterations to the individual sub-clonal tumour cell populations. Here we show that ctDNA can inform on tumour heterogeneity and evolution of sub-clones in patients. In one experiment, we were able to track the levels of mutations determined to be unique to two mutually exclusive sub-clones. We observed the decline in VAF of mutations associated with one sub-clone, and the increase in VAF of mutations associated with the second, likely resulting in the expansion of this sub-clone. We showed ctDNA provided an accurate representation of the mutations observed in tumour, and in one patient, showed liquid biopsies were less limited in spatial heterogeneity assessment than solid tumour biopsies. We observed several cases with convergent evolution of tumour sub-clones to acquire distinct mutations affecting the same gene allowing survival during treatment. These cases provide a means to track the changes in VAF of mutations existing in individual sub-clones.

3.2. Introduction

In the previous chapter, I highlighted the need to test multiple target mutations within a patient when tracking ctDNA change over time. Here, I continued to study the importance of utilizing multiple target mutations when detecting ctDNA within a patient. I performed amplicon sequencing on patients from the JGH (separate from the QCROC cohort) and hybridization capture on patients from BC Cancer Agency (BCCA cohort), targeting multiple target mutations for each patient to observe changes in ctDNA over time. I sought to compare ctDNA changes with the changes in disease progression (relapse) in these patients.

In the separate patients from JGH that were selected for this analysis based on the availability of samples and the presence of high ctDNA (namely, PT419 and PT255),

we generated WES data from normal, diagnostic and relapse samples and selected suitable target mutations to track in ctDNA from five and six plasma samples. Patient 419 had *de novo* DLBCL and relapsed after initial chemotherapy treatment. Tumour biopsies were obtained from diagnosis and relapse 15 months apart, with plasma samples obtained throughout this time (Figure 3.1A). I performed targeted amplicon sequencing on plasma to track ctDNA during the course of treatment, and on tumour for comparison. Patient 255 had aggressive DLBCL with features of Burkitt lymphoma (commonly described as B-cell lymphoma unclassified or BCLU). The patient was given R-CHOP and high dose chemotherapy but showed no clinical response to this treatment (chemo-refractory) and quickly relapsed (relapse 1). After further treatment, the patient underwent a second relapse (relapse 2) 10 months after diagnosis and CTCs and serial plasma samples were obtained from blood collected at this time, which I used for WES and targeted amplicon sequencing, respectively. The patient became pancytopenic from the chemotherapy during this time and relapsed a third time (relapse 3) 30 days subsequent to relapse 2. CTCs were obtained from blood collected at the time of relapse 3 and were subjected to WES (Figure 3.1B).

Analysis of WES data from matched normal and tumour samples identified several somatic mutations as potential targets for monitoring ctDNA. Notably, we observed a set of mutations that were only detectable in the diagnostic tumour sample, and a set of mutations only detectable in the relapse tumour sample(s), an example of temporal heterogeneity in the tumour. The presence of relapse-specific mutations suggests the patient acquired these mutations sometime after diagnosis, during the course of treatment, or that they were sub-clonal at the time of diagnosis. In scenarios such as this, some of the relapse-specific mutations could be relevant in treatment resistance. This is promising for our ctDNA analysis because having sets of mutations unique to each time point allowed us to develop assays to track levels of VAF for diagnostic- and relapse-specific mutations, and determine the time point we first detect the rise or decline of either sets of mutations. These experiments assess the utility of ctDNA to inform on temporal heterogeneity.

Currently, clinicians utilize techniques such as tumour biopsies and CT scans to monitor a patient's disease and tumour progression. These techniques have its downsides, such as invasiveness of biopsies and costs involved with CT scans. CtDNA provides a non-invasive, cost-effective means to monitor tumour progression. Therefore,

it is important to show ctDNA is capable of representing the tumour genome as accurately as an actual tumour biopsy. We perform hybridization capture on a series of NHL patients (BCCA Cohort) testing DNA from tumour and ctDNA from plasma. In multiple cases, we show analysis of ctDNA depicts the mutations observed in tumour samples.

One major limitation of using tumour biopsies is the lack of access to cells from other sites and thus a limited ability to evaluate spatial heterogeneity. NHLs are typically disseminated across multiple sites (e.g. lymph nodes) at the time of diagnosis. It is plausible that this spatial spread doesn't equally affect all sub-clones such that distinct populations are more or less well represented among the sites. CtDNA may overcome this limitation, as collected plasma can contain DNA contributed from tumour cells in any anatomical site. The VAF of mutations in tumour samples will be different from the VAF of mutations in plasma due to spatial heterogeneity and variable contribution of non-tumour DNA in either sample. Therefore, it is unlikely that ctDNA analysis will show identical or similar VAF of mutations compared to the reported VAF of the same mutations from experiments using tumour samples. However, it is still important to determine the utility of ctDNA to reflect the same observed mutations as detected in tumour samples. Such data could lend support to the utility of liquid biopsies to select target mutations as an adjunct to tumour biopsies for studies where tumour biopsies may be unobtainable at later time points.

Driver mutations, by definition, confer a selective advantage to a tumour clone and a subset (or possibly unique set) of drivers could be relevant in the context of the selective pressure of chemotherapy treatment. A clone that gains such a mutation can undergo clonal expansion to become a sub-clone population. Expectedly, different sub-clones may gain similar mutations within the same microenvironment driving selection. This "convergence" towards mutations in the same gene in different sub-clones can be described as convergent evolution. This process is difficult to identify and verify through ctDNA analysis. However, observing mutations affecting a similar region in a driver gene that follow different trends in VAF change across time, would suggest those mutations were specific to unique sub-clones undergoing different rates of change within the clonal structure. In these cases, ctDNA can be used to sufficiently monitor expanding or declining sub-clones, to inform on tumour dynamics during the course of treatment.

In patients with low or undetectable ctDNA, we cannot be certain if there is a lack of ctDNA, or if the target mutations identified from tumour biopsy data was incomprehensive. That is, there may be targetable mutations not detected in tumour that would readily detect ctDNA. This may occur in patients where the tumour biopsy was obtained in an earlier time, and the clonal structure had since changed, with new tumour sub-clones contributing the majority of ctDNA in the plasma sample. Alternatively, ctDNA may harbour target mutations observed in a low VAF from tumour biopsy due to spatial heterogeneity. These low VAF mutations identified by WES of tumour are not often selected as target mutations to test in ctDNA. Identification of novel mutations from sequence analysis of ctDNA may provide quantification of ctDNA and changes in ctDNA across different time points without reliance on data from tumour samples.
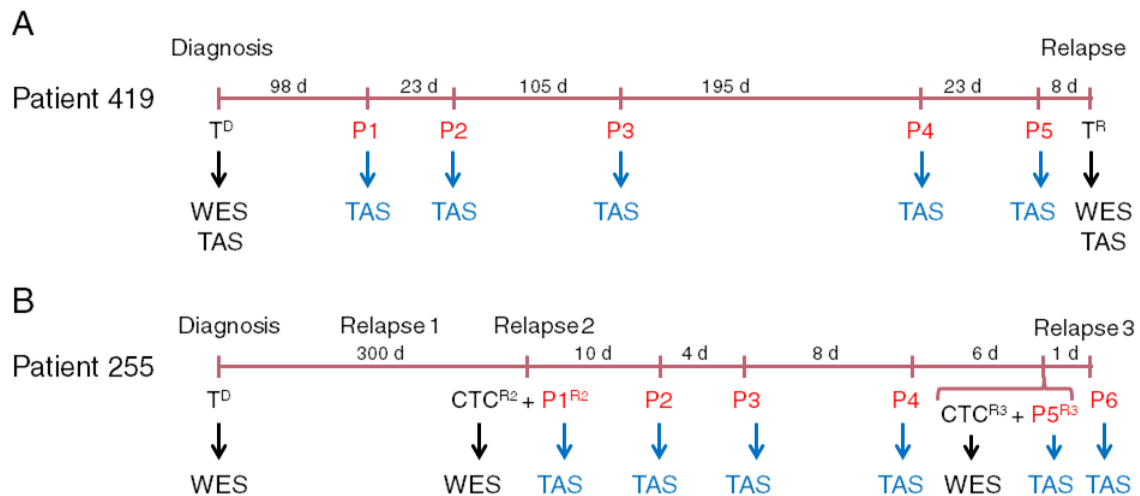
Figure 3.1.   Timeline of two patients from JGH
Shown here is the time between samples taken from two NHL patients from JGH. T^D: diagnostic tumour sample, T^R: relapse tumour sample, P: plasma sample, CTC^R: circulating tumour cells from relapse, d: days, WES: whole exome sequencing, TAS: targeted amplicon sequencing. (A) Patient 419 had five plasma samples (P1 to P5) obtained between tumour biopsies at diagnosis and relapse. Plasma samples were used for TAS and tumour samples were used for WES and TAS. (B) Patient 255 had six plasma samples (P1 to P6) obtained between relapse 2 and relapse 3, used for TAS. WES was performed on diagnostic tumour biopsy and CTCs from relapse 2 and relapse 3.

3.3. Materials and Methods

3.3.1. DNA extraction

The patient samples and data studied in this chapter were obtained from collaborators at Jewish General Hospital (JGH) in Montreal, QC, and from the BC Cancer Agency (BCCA) in Vancouver, BC. DNA was extracted from plasma received from JGH and BCCA following the protocol outlined in Section 2.3.1. The plasma samples from JGH were collected in tubes with EDTA which acts as an anti-coagulant, and has less effect on PCR than Heparin (used only with samples from Chapter 2). Samples from BCCA were obtained as whole blood in Streck BCT® (blood collection tube), which were designed to stabilize nucleated blood cells and minimize HMW DNA contamination. I processed whole blood samples, to separate plasma (typically 10 mL volume), buffy coat, and red blood cells, using the Blood and Plasma Processing and Storage protocol (Centre for Translational and Applied Genomics, PHSA).

I extracted cfDNA from thawed plasma samples using the QIAamp® Purification of Circulating Nucleic Acids from Serum or Plasma kit (Qiagen), as detailed in Section 2.3.1. Plasma samples from JGH patients ranged from 0.5 to 2 mL volumes, depending on sample, and PBS was added to samples with less than 2 mL to maximize efficiency. I used up to 5 mL volume for plasma samples prepared from whole blood processing of BCCA patients, as plasma was not a limiting factor in this cohort.

3.3.2. Library preparation and hybridization capture

Library preparation of plasma samples using our custom barcoded adapters was performed as described in Section 2.3.3, with one major change: The NEBNext® Ultra™ II DNA Library Prep kit (New England Biolabs) was used instead of the KAPA Low Throughput library preparation kit (Roche). Using the NEB kit, several steps in the library preparation process including end-repair and A-tailing reactions could be performed in one tube using one aliquot of AMPure XP beads (Agencourt) for purification. This improved our cost-efficiency and speed for the library preparation step in the experiment.

I used an input of 25 ng of DNA from plasma and tumour for these experiments. DNA from tumour samples were sheared to 200-300 bp fragments using a Covaris®

58

M220 focused ultrasonicator (Thermo Fisher Scientific). Library preparation of DNA from tumour followed the same protocol as plasma, except normal Y-shaped TruSeq adapters were used instead of our custom adapters. The TruSeq adapters are similar in sequence to our custom adapters, lacking only the 5 degenerate bp molecular barcode and 3 bp fixed tag unique to our custom adapters. TruSeq adapters were used for tumour samples in part due to cost, and because tumour samples typically had high mutation VAF, and did not require single molecule identification.

Hybridization capture and library sequencing was performed as described in Section 2.3.4. For sequence data from experiments on tumour, FASTQ files generated by the MiSeq were used to align to the hg19 reference genome (GRCh37) using BWA (http://bio-bwa.sourceforge.net/) and aligned sequences were visualized in IGV (http://software.broadinstitute.org/software/igv/) to determine mutant and wildtype reads used to calculate the VAF.

3.3.3. ProDuSe

ProDuSe is a python based toolkit used to build consensus sequences from raw sequence reads sharing the same molecular barcode, which we analyze to determine the count of individual molecules supporting a variant of interest. Additionally, ProDuSe has a built-in SNV caller (snv.py), which runs a pileup through the final BAM file to determine the number of bases supported by both positive and negative strands of an individual molecule. Positions that had support in a non-reference base were considered an SNV. The raw output containing this information is likely filled with sequence artifacts and false positives, hence, the output is filtered. For these experiments, we added a strand bias filter of 0.2, a variant allele fraction filter of 0.01 and an alternative base count filter of less than 5. We defined "duplex support" of SNVs as the presence of a non-reference base seen in two collapsed reads from an individual molecule, and filtered SNVs with duplex support were manually curated to assess validity and novelty.

3.4. Results

3.4.1. Discovery of relapse-specific mutations in NHL patients

PT419 was diagnosed with *de novo* DLBCL and relapsed within 15 months of diagnosis. From WES data of the diagnostic and relapsed tumour biopsy, I picked seven target mutations that were determined to be either diagnostic-specific (unique to diagnostic tumour biopsy) or relapse-specific (unique to relapse tumour biopsy). Using targeted amplicon sequencing, I successfully detected ctDNA using target mutations in *NOTCH1*, *ATG16L2* and *PSMC3*. Amplicon sequencing was performed on the diagnostic and relapse biopsy, and on extracted DNA from the five plasma samples (Figure 3.2). I confirmed the *NOTCH1* mutation was present in both tumour biopsies, which is useful as a measure of ctDNA for each sample. Additionally, the *ATG16L2* mutation was only observed in the diagnostic biopsy (diagnostic-specific) and the *PSMC3* mutation was only observed in the relapse biopsy (relapse-specific). In the first two plasma samples (P1 and P2), I observed the *NOTCH1* mutation at a VAF of 0.0089 and 0.0114. However, there was no support for the *ATG16L2* mutation at these, or at any subsequent plasma time points. The *PSMC3* mutation was also undetectable at P1 and P2. However, we observed an increase in *PSMC3* mutation to a detectable limit by P3 which maintained its trajectory by P4 and P5.

For PT255, we had WES data from tumour samples at diagnosis and from CTCs at relapse 2 (10 months after diagnosis), and from CTCs at relapse 3 (29 days after relapse 2). I picked a set of target mutations and applied amplicon sequencing to six plasma samples taken sequentially after the relapse 2. Using this approach, I was able to successfully detect ctDNA in 17 target mutations, and tracked these across 29 days after relapse 2 (Figure 3.3). Target mutations were grouped into three separate categories: diagnostic, relapse 2, and relapse 3.

Diagnostic target mutations (blue) consisted of mutations in *ID3*, *RTN1*, and *TP53*. The VAF for these mutations stayed relatively similar across all plasma time points. Relapse 2 target mutations were mutations detected only in the CTCs at relapse 2 from WES. These consisted of mutations in *DDR2*, *PPP1CA*, *NUP210*, *ZNF45*, *LRP1*, and *URB2* (red). Amplicon sequencing of all six plasma samples showed that the VAF of these mutations slowly declined to undetectable limits 29 days after relapse. An

additional relapse 2 target mutation, an insertion in *MS4A1* (orange), was also included with these relapse 2 target mutations that declined to an undetectable VAF. The last category, relapse 3 target mutations, consisted of mutations in *SBK1*, *SCMH1*, *OCA2*, *OXTR*, and *INPP4B* (green). Amplicon sequencing of all six plasma samples showed that the VAF of these mutations increased from very low levels early after relapse to the same level of VAF as the diagnostic target mutations that stayed level throughout all time points. Also included in the relapse 3 target mutations is a separate *MS4A1* missense mutation (orange) that followed the same VAF trend as the other mutations in this category.
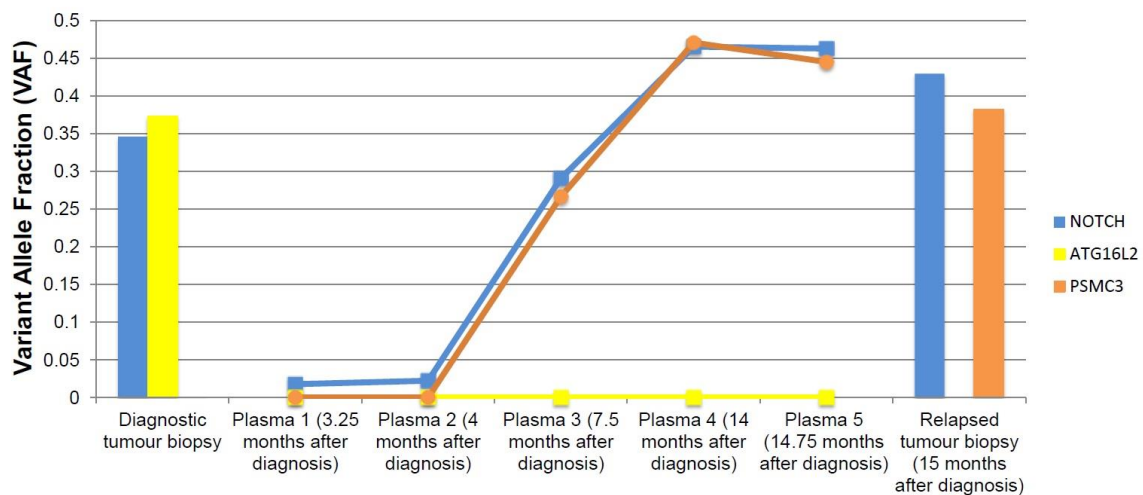
Figure 3.2.   Targeted amplicon sequencing results from DLBCL patient 419
Results from three target mutations (*NOTCH1*, *ATG16L2*, *and PSMC3*) are shown. Bar graph shows the VAF of these mutations at diagnostic and relapse tumour biopsies (15 months apart). Line graph shows the changes in VAF of these mutations across five plasma samples intervening the tumour biopsies.
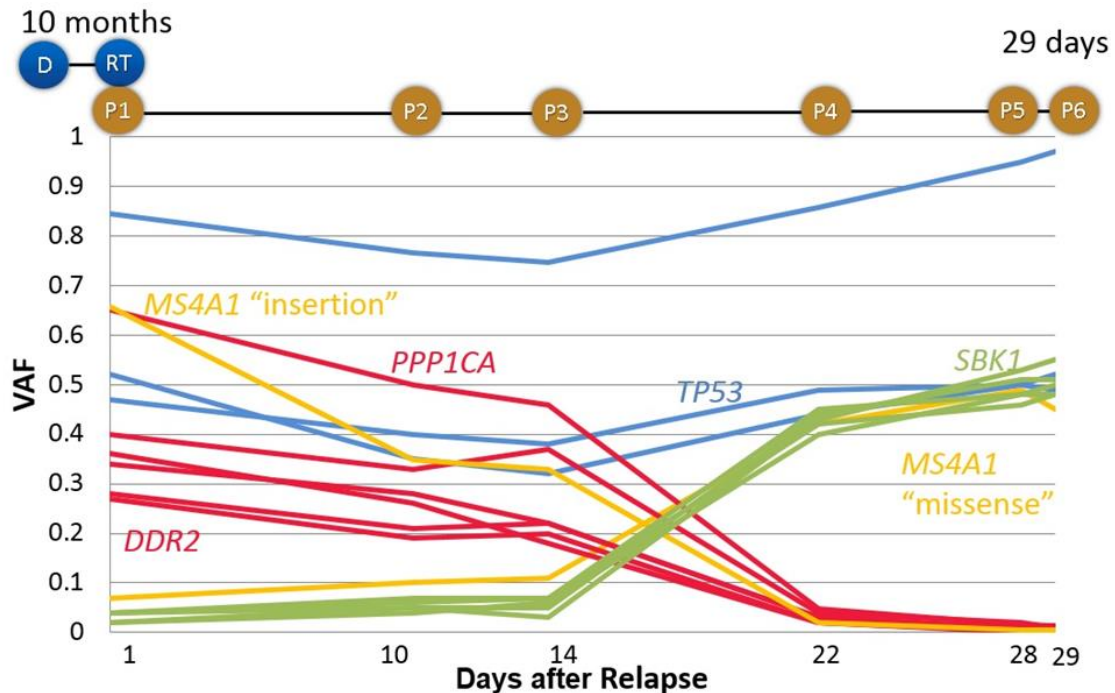
Figure 3.3.   Targeted amplicon sequencing results from BCLU patient 255
Line graph showing results from targeted amplicon sequencing across six plasma time points (P1 to P6) taken sequentially after relapse 2 (RT). VAF of diagnostic mutations (blue) remained constant, whereas VAF of relapse-specific mutations (red and orange) decreased over time, with the exception of one mutation (*MS4A1* "missense") that increased. We assayed ctDNA associated with mutations from that sub-clone (green) which showed a consistent pattern with the expanding relapse-specific mutations. D: tumour at diagnosis.

3.4.2. Hybridization capture on BCCA cohort

We obtained tumour and plasma samples from seven NHL patients undergoing treatment at the BC Cancer (BCCA cohort). We were provided with a diagnostic tumour biopsy and a plasma sample collected between 4 months and 7 years after diagnosis, depending on the patient. I performed hybridization capture using the IDT HME pool and IDT EXLYM pool on both diagnostic tumour and plasma sample. These patients comprised three DLBCLs, one mantle cell lymphoma (MCL) and two low-grade follicular lymphoma (FL). Four of the seven patients had undetectable ctDNA despite sufficient read depth across target mutations and successful hybridization capture on tumour DNA in these patients (Table 3.1). It is unclear why these patients had undetectable ctDNA, despite two patients having relapsed from their disease (BC19 and BC22). Using larger amounts of input DNA could have improved sensitivity to detect ctDNA in all these cases.

In the remaining three cases with detectable ctDNA (BC12, BC04 and BC02), the levels were sufficiently high to facilitate direct assessment of mutations represented at diagnosis. All three cases showed mutations in ctDNA that still persisted since diagnosis, which varied from 1 to 4 years prior depending on patient (Figure 3.4). In two of these cases (BC12 and BC04), several mutations detected in tumour remained represented in the plasma. In BC12, mutations such as *TP53* and *CARD11* remained present at relatively high VAF levels, and are likely "diagnostic" mutations associated with a CPC (Figure 3.4A). The plasma for this patient was obtained four years after diagnostic biopsy, and showed the relative levels of a *CD58* mutation (large deletion) had declined to a VAF of zero (yellow), and that two new *CD58* mutations (green) and a *MYD88* mutation (purple) not detected in tumour was prevalent at a relatively high VAF. Interestingly, BC12 was reported to have disease progression (classified as a non-responder) one month *after* the plasma sample was obtained. BC04 did not show signs of disease progression (classified as a responder), but interestingly, target mutations in *MEF2B* and *TP53* were still detectable in ctDNA (Figure 3.4B). The decline in VAF of *TP53* relative to *MEF2B* may suggest the sub-clone associated with *TP53* mutation became less prevalent compared to the sub-clone associated with *MEF2B*.

BC02 was another non-responding patient, and had plasma obtained four years after diagnosis, although disease progression was reported one month *before* plasma draw. This is the only case from the BCCA cohort where we analyze ctDNA shortly after a relapse had occurred. I observed a decline in target mutations *CREBBP and FOXO1* to a relatively lower VAF, and several other target mutations such as *BCL2, MLL2 (KMT2D) and EZH2* disappeared with a VAF of 0 (Figure 3.4C). These target mutations are likely associated with a sub-clone or sub-clones that may have declined since the tumour biopsy was obtained. Notably, I observed the presence of a *TP53* mutation (pink) with relatively high VAF compared to the other target mutations in ctDNA, which was detectable at a relatively low VAF in the tumour biopsy. It is likely the *TP53* mutation is associated with a sub-clone that had expanded to become dominant in the clonal structure in this patient.
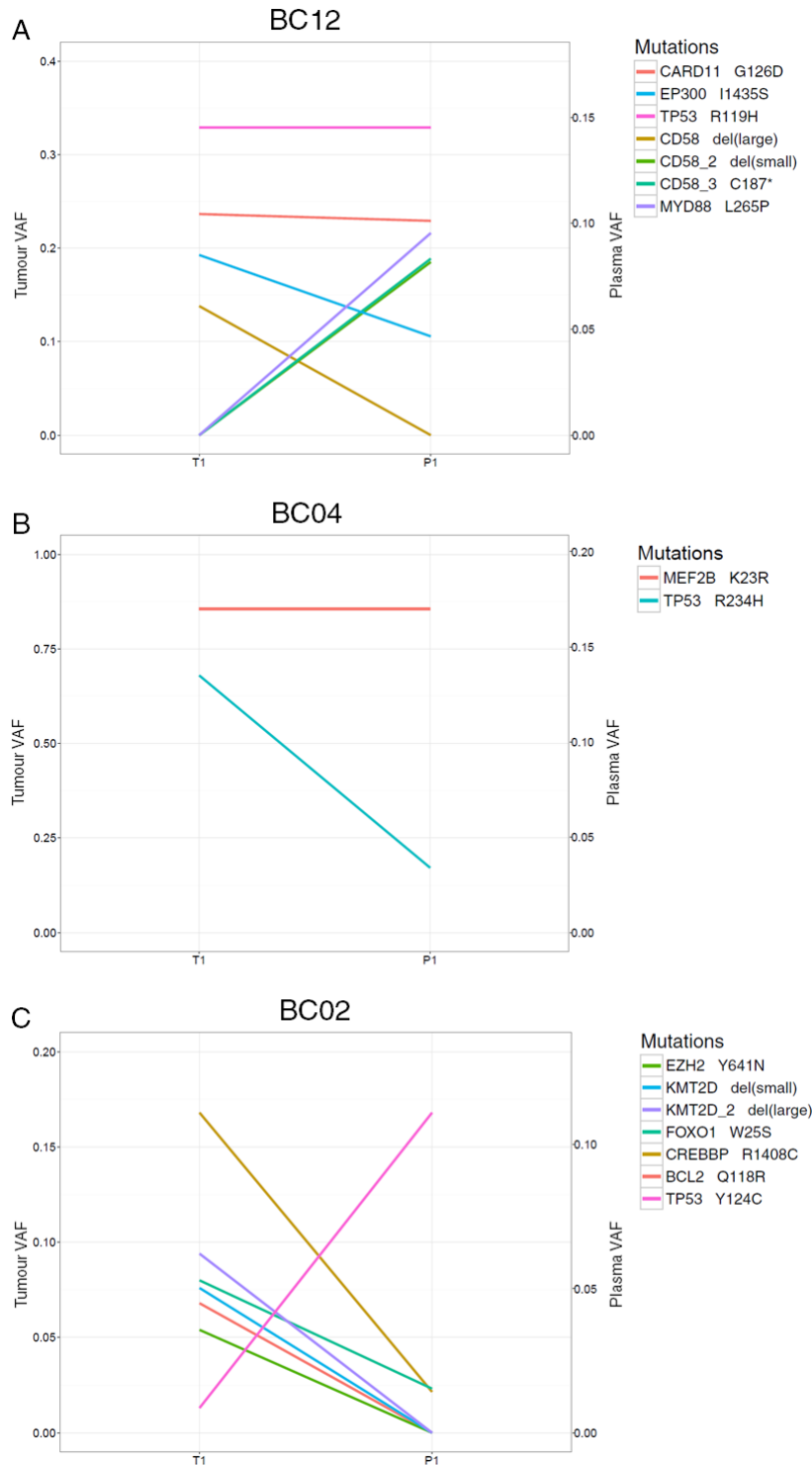
Figure 3.4.   Hybridization capture of tumour and plasma from 3 NHL patients
(A) BC12 had plasma (P1) obtained 4 years after the diagnostic biopsy (T1), showing outgrowth of mutations in *CD58* and *MYD88*. (B) BC04 had plasma (P1) obtained 1.5 years after the diagnostic biopsy (T1), and mutations detected in tumour remain represented in plasma. (C) BC02 had plasma (P1) obtained 4 years after the diagnostic biopsy (T1), showing outgrowth in a *TP53* mutation.

Table 3.1.   VAF and coverage data on tumour and plasma from BCCA patients

Patient	Diagnosis	Gene	Amino acid change	VAF in tumour	Coverage	VAF in plasma	Collapsed reads
BC12	DLBCL	CARD11	G126D	0.236	444	0.101	425
		EP300	I1435S	0.193	436	0.047	343
		TP53	R119H	0.329	465	0.145	296
		CD58	large del	0.138	181	0.000	211
		CD58	Frameshift Del	0.000	241	0.082	292
		CD58	C187*	0.000	362	0.083	192
		MYD88	L273P	0.000	494	0.095	241
BC04	MCL	MEF2B	K23R	0.856	174	0.170	74
		TP53	R234H	0.680	1703	0.034	439
BC02	DLBCL	EZH2	Y641N	0.054	405	0.000	373
		KMT2D	Frameshift Del	0.076	799	0.000	551
		KMT2D	Frameshift Del	0.094	615	0.000	416
		FOXO1	W25S	0.080	1007	0.015	196
		CREBBP	R1408C	0.168	339	0.014	352
		BCL2	Q118R	0.068	545	0.000	288
		TP53	Y124C	0.013	796	0.111	252
BC06	DLBCL	BCL2	L175Q	0.107	866	0.000	449
		EZH2	Y641S	0.142	330	0.000	566
		IRF8	I424T	0.113	576	0.000	611
		MEF2B	D83V	0.161	385	0.004	553
		PIM1	L88V	0.313	895	0.004	250
		TBL1XR1	Y446S	0.248	645	0.000	828
BC16	COM	CREBBP	Frameshift del	0.022	455	0.000	462
		SOCS1	I67S	0.058	416	0.004	250
		STAT6	E267G	0.075	464	0.000	424
		B2M	L12P	0.068	219	0.000	122
BC19	FL	MLL2	Frameshift del	0.412	271	0.000	372
		BCL2	F49S	0.312	443	0.000	263
		EBF1	N172D	0.428	355	0.000	445
		CREBBP	H1449Y	0.406	414	0.000	355
		EZH2	A687V	0.525	438	0.000	289
		MLL2	Q4387*	0.278	486	0.000	424
BC22	FL	MLL2	Frameshift del	0.480	220	0.000	395
		MLL2	L3325*	0.132	394	0.003	371
		BCL2	A77G	0.324	293	0.000	235
		CREBBP	I1445S	0.303	300	0.000	261
		HIST1H1E	G91D	0.315	238	0.000	206

3.4.3. Convergent evolution of driver mutations in sub-clonal populations

We had previously seen a case (PT255) where different mutations affect the same gene. The two mutually exclusive sub-clones that harboured different *MS4A1* mutations resulting in the same downstream effects, is an example of convergence in mutations of sub-clones towards a specific gene. I observed this phenomenon again from hybridization capture of BC12, where the patient showed the presence of multiple *CD58* mutations, two of which were unique to plasma and one was only seen in tumour (Figure 3.5A). The large deletion (1115 bp length) of *CD58* was first detected at diagnosis in the tumour sample (purple), however this mutation disappeared by the plasma time point (4 years later). Although the sub-clone associated with this *CD58* mutation had declined, mutations in the *CD58* gene still persist in the plasma. I observed two new *CD58* mutations, a nonsense mutation (red) and an 8 bp deletion (green), in roughly equal proportion.

I observed a similar case in a QCROC patient from an earlier experiment (PT39). This patient harboured ten different target mutations detected by hybridization capture. Additionally, this patient had three unique mutations affecting *TMS4BX*, which was detectable in tumour and plasma samples obtained from both day 0 and day 15 time points (Figure 3.5B). Comparing changes in these mutations between time points within the tumour shows the proportional representation of these mutations remain consistent. However, the large deletion that affects the start codon (green) was observed at a higher proportion in tumour compared to plasma. In plasma, the remaining two deletions, a small 2 bp deletion (red) and a large 61 bp deletion (purple), are observed at a higher proportion. Notably, we observe changes in this proportion from day 0 to day 15 in plasma, where the small 2 bp deletion (red) decreases and the large 61 bp deletion (purple) increases.
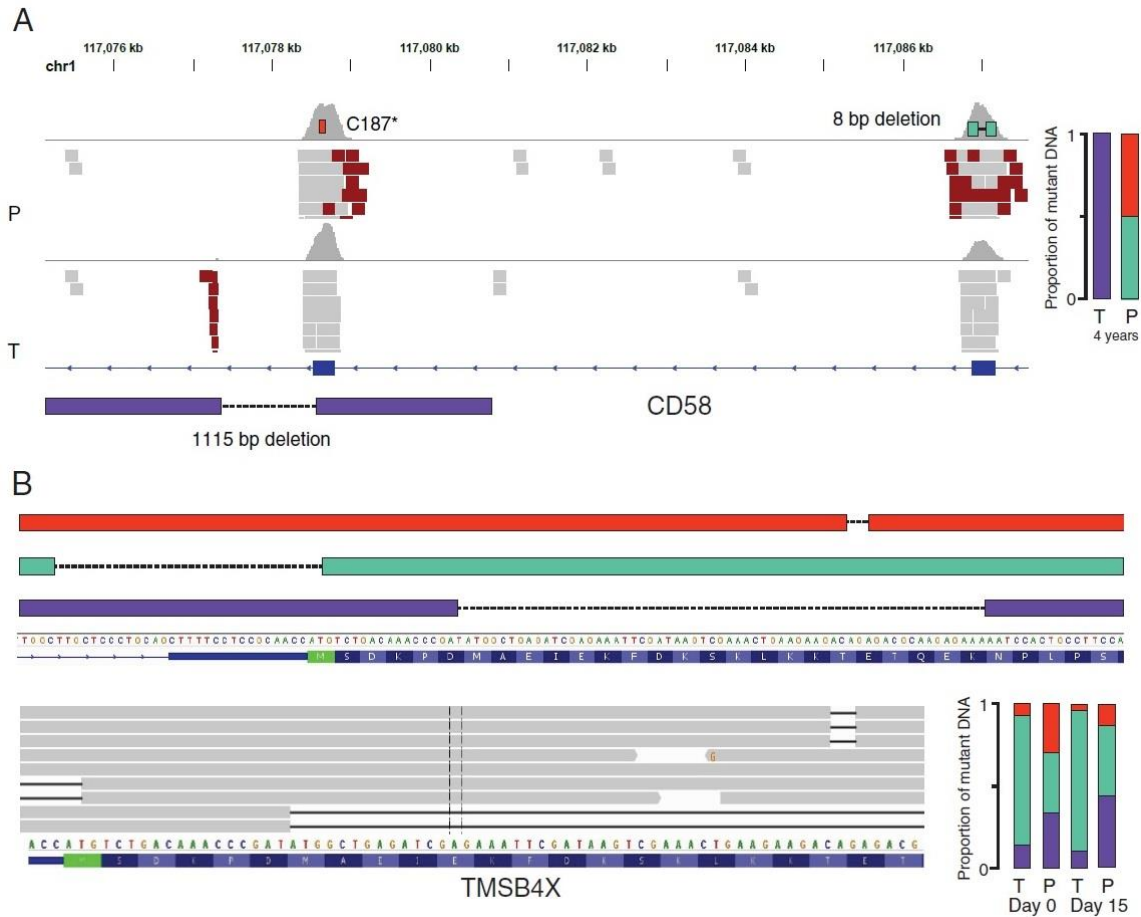
Figure 3.5.   Two cases of convergent evolution towards gene mutations
Analysis of deletions in ctDNA showing mutations affecting the same gene as an example of convergence of gene mutations within a patient. (A) In BC12, we observe three separate mutations: 1115 bp deletion (purple), C187* nonsense mutation (red), and 8 bp deletion (green) in *CD58*. Plasma (P) was taken 4 years after tumour biopsy (T) and the proportion of ctDNA is shown on the right. (B) In PT39, we observe three separate deletions in *TMSB4X*: small (red) and large (purple) deletions affecting the same exon, and a large (green) deletion that truncates the AUG start codon. T: Tumour, P: Plasma.

3.4.4. Discovery of novel variants

Using the SNVcaller in ProDuSe, I am able to query all the mutations reported in a patient. Mutations with VAF higher than 0.01 from collapsed (single molecule) reads and had duplex support were manually curated to identify potentially real mutations. I discovered the presence of two new mutations not detected previously in tumour for PT07 (Figure 3.6). PT07 was a non-responder that showed an insignificant decrease in mean VAF. A mutation in *TP53* (green) follows the expected trend we determined in Chapter 2 for the mean VAF of this patient. However, a novel variant discovered in *MLL2*

(brown) was shown to increase significantly from day 0 to day 15. This mutation could be associated with an expanding sub-clone.

I performed a similar analysis on PT11, a non-responder showing discordance in ctDNA analysis. The results for this patient also show evidence for multiple sub-clonal populations (Figure 3.7). Of the novel variants, *TNFRSF14* exhibited proportionally similar decreases in VAF compared to other variants reported in Chapter 2. However, a separate set of mutations increased in prevalence relative to these (*FOXO1*, *MYC*, and *EBF1*). Interestingly the new *MYC* variant (F153L, purple) had minimal support in the initial plasma sample, but increased to detectable levels in the day 15 sample. This is another example of convergent evolution whereby the sub-clone associated with the P74A *MYC* (yellow) was replaced by another sub-clone with a separate mutation in the same gene.
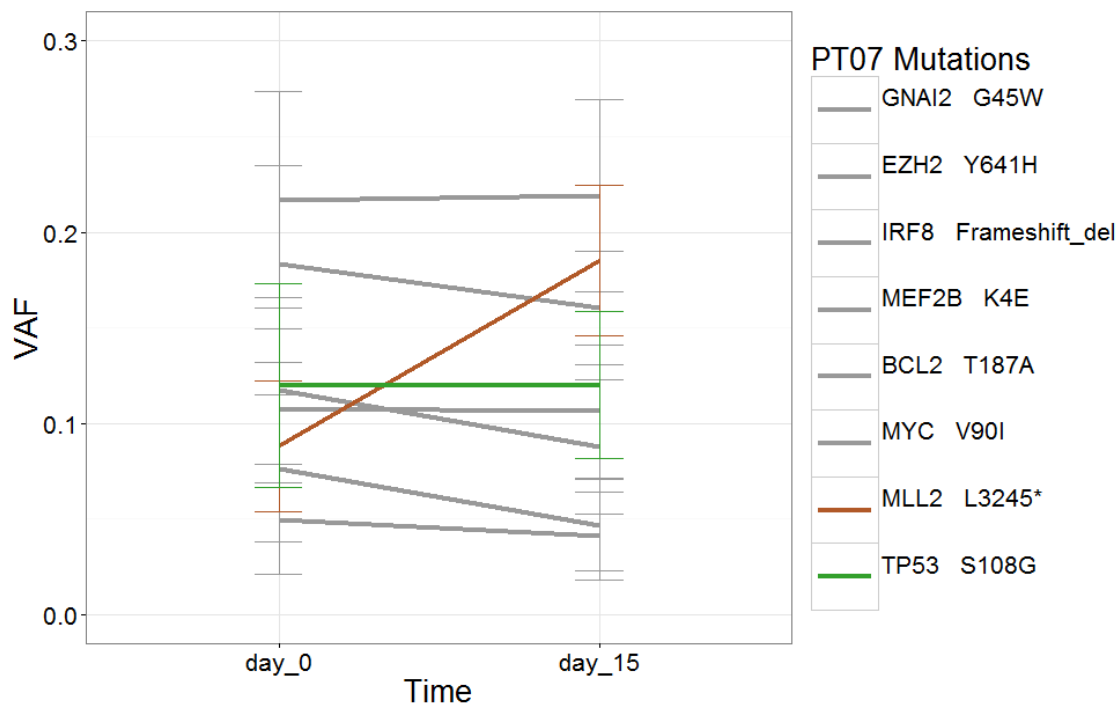
Figure 3.6.   Novel variants detected in PT07
The SNVcaller of ProDuSe was used to identify novel variants in PT07 overlaid on previously detected variants from Figure 2.10B. Old variants are "grayed out", and the two new variants, *MLL2* and *TP53* are shown in brown and green, respectively.

68
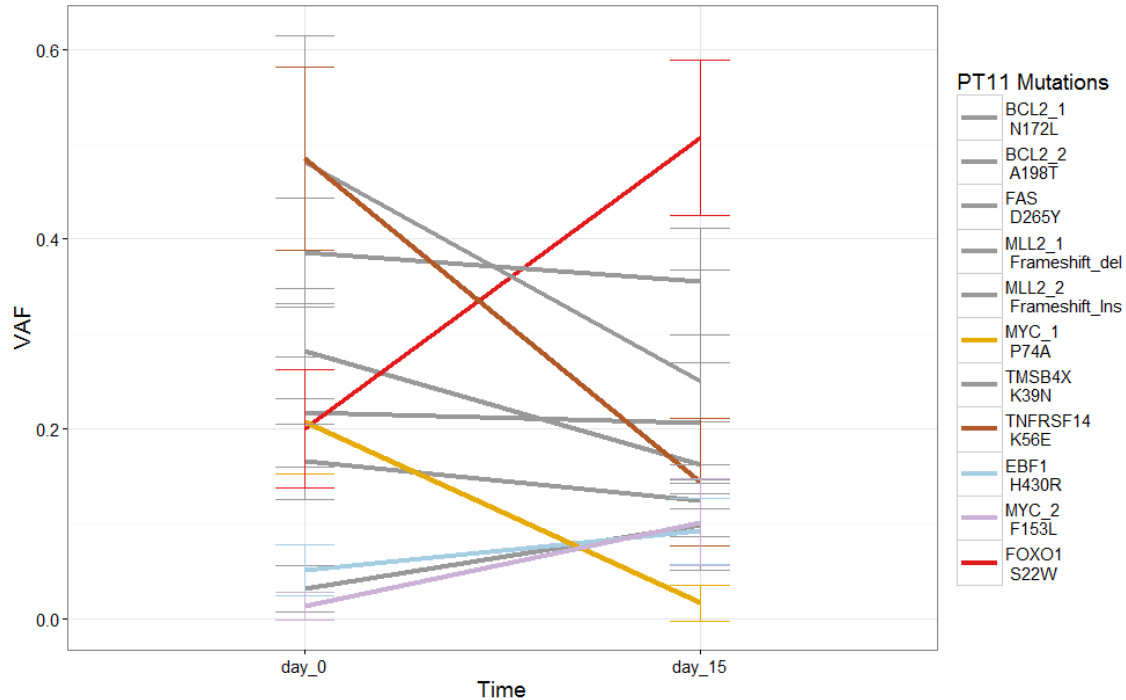
Figure 3.7.   Novel variants detected in PT11
The SNVcaller of ProDuSe was used to identify novel variants in PT11 overlaid on previously detected variants from Figure 2.10D. Old variants, except MYC_1, are "grayed out", and four new variants, *TNFRSF14, EBF1, FOXO1 and a new MYC* are shown.

3.5. Discussion

Patient 419 had *NOTCH1* mutation at low VAF in the early plasma samples, suggesting ctDNA was low but detectable. This is important to confirm the complete absence of *ATG16L2* and *PSMC3* mutation, which was well below 0.01 VAF and thus considered undetectable. This suggests the *ATG16L2* mutation was specific to a tumour clone that had already decreased in abundance or became extinguished by this time. The sudden increase of *PSMC3* mutation at plasma 3 suggests this mutation arose in the intervening time prior to this plasma draw, suggesting the *PSMC3* mutation was present in the dominant clone after this time point and beyond. This patient is a good example of branched evolution, where these two sub-clones derived from a CPC.

Patient 255 was interesting as we observed the presence of two separate mutations within one gene, *MS4A1*. *MS4A1* encodes the surface phosphoprotein CD20 on B-cells, and is a known target of rituximab from R-CHOP chemotherapy. *MS4A1* mutations involving the rituximab epitope on exon 5, although rare, drive resistance to R-CHOP[123]. We detected a frameshift insertion mutation affecting exon 5 and a missense

mutation affecting exon 4, both believed to independently inhibit interaction of rituximab and CD20. I observed the *MS4A1* insertion mutation and the other relapse 2 target mutations slowly decline in VAF from plasma 1 time point (shortly after relapse 2) through to plasma 6 time point (relapse 3, which was 29 days after relapse 2), indicating the decline of the sub-clone associated with the relapse 2 target mutations. Concurrently, I observed the *MS4A1* missense mutation, along with the other relapse 3 target mutations, increase in VAF from plasma 1 to plasma 6, indicating the expansion of a new sub-clone associated with the *MS4A1* missense mutation and likely the culprit of this patient's second relapse. It is certain that the two *MS4A1* mutations were associated with mutually exclusive sub-clones, as it is unlikely we would see two mutations affecting the same region in a gene in one sub-clone. Due to the convergent evolution towards *MS4A1* mutation by these two sub-clones in this patient, we were able to observe a change in tumour heterogeneity in this patient, as one sub-clone expanded to take over.

Hybridization capture experiments on the BCCA cohort provided evidence for the utility of ctDNA to allow detection of mutations known to be present in a matched tumour sample (given sufficiently high ctDNA). BC12 and BC04 are good examples as the majority of mutations from the diagnostic tumour biopsy were still present in the plasma that was collected at a later date. Although the relative VAF of these mutations may differ between tumour and plasma, it is important that the observed mutations in tumour are reflected in plasma. This supports the utility of ctDNA as a substrate to determine the landscape of mutations in a patient, and could offer an alternative to tumour biopsies for mutation profiling applications. In patients such as BC02, it is difficult to determine if a decline in relative VAF of a certain set of mutations is a consequence of the decline of a sub-clone, or if ctDNA did not reliably represent that set of mutations. Considering the time difference between obtained tumour and plasma samples in this patient (4 years), it is more likely that a declining sub-clone contributed to the decrease in relative VAF. Further experiments to compare the representation of mutations in tumour and plasma should be done on patients where tumour and plasma samples are obtained with less intervening time. Combining clinical data and ctDNA analysis of BC02 suggest the increase in *TP53* was associated with a sub-clone that expanded resulting in disease progression of this patient (relapse).

The limit of detection (LOD) for hybridization capture experiments varies due to many factors such as the size of the capture space and depth of sequencing. We must

determine the number of expected copies per loci (genome equivalents, GE) in our starting input of 25 ng DNA. Assuming 3.3 pg per haploid genome equivalent, 25,000 pg / 3.3 pg = 7,576 copies per locus are expected. Typically, the recovery efficiency of these capture experiments are such that approximately two thirds of the cfDNA fragments are lost. Therefore, in an ideal case, we have 2500 GE captured at regions at the highest depth. Conservatively, I estimate this to be closer to 2000 GE with optimal conditions. For our experiments, we require duplex support of an SNV, so 2 of the 2000 GE must form a consensus at an SNV. The LOD in this hypothetical scenario with excellent conditions is 0.1%. In cases with undetectable ctDNA, such as the four BC patients from Table 3.1, the amount of collapsed reads were much lower than the estimate of 2000 GE (average number of collapsed reads: 387.2), and the LOD is closer to 0.5% (VAF of 0.005). One potential solution for this problem is to increase the starting input to at least 100 ng of DNA, especially in cases such as these from the BCCA cohort where DNA from plasma was not a limiting factor. Alternatively, deeper sequencing of the final libraries can also improve sensitivity in these cases. The estimated 2000 GE is dependent on sequencing the library to at least 2.5 million sequence reads depth (~10% of a MiSeq run).

We observed more evidence of convergent evolution in BC02, where the detection of three different *CD58* mutations suggested the presence of at least two sub-clones in the clonal structure of this patient. The two *CD58* mutations seen in plasma (C187* and the 8 bp deletion) may exist in one sub-clone affecting the same or both alleles. Regardless, it was clear that the large *CD58* deletion was associated with a sub-clone that declined, while at least one other new sub-clone (and the associated *CD58* mutations) expanded. In our last example of convergent evolution, we observed three different mutations in *TMSB4X* in non-responder PT39. These mutations were likely associated with three different sub-clones, evidenced by dissimilar changes in the VAF for each mutation between plasma time points. However, there was no evidence for any of these sub-clones declining in this patient. Strikingly, the proportion of these mutations was different between tumour and plasma samples from one time point. We observe a much higher proportion of the "green" deletion in tumour compared to plasma (Figure 3.5B). This suggests the sub-clone associated with the "green" deletion affecting the start codon of *TMSB4X* was more prevalent in the tumour biopsy. These cases are likely scenarios where different sub-clones undergo convergent evolution towards mutating

71

the same gene to provide survival capabilities during treatment. By tracking the levels of different mutations affecting the same region of a gene, these situations manifest as a divergent rise and decline of the VAF for the mutations existing in distinct sub-clones. Although these examples provide support for the utility of ctDNA to inform on the clonal structure of a tumour, this is not a reliable method as convergent evolution in sub-clones may not occur in every patient. Further studies on ctDNA may lead to a more effective method for assessing clonal structure. The example in PT39 supports the use of liquid biopsies to assess spatial heterogeneity over tumour biopsies, however more tests are needed to determine if ctDNA can provide a better representation of sub-clones across all tumour sites in this patient. Experiments with multiple tumour biopsies from different lymph nodes in conjunction with ctDNA analysis to test spatial heterogeneity may provide more support, although finding a patient to enroll in such a study will be difficult.

The utility of novel variant discovery showed promise for resolving discordant cases. PT11 showed significant decrease in mean VAF suggesting a decline in tumour burden, though clinical results suggested the opposite. The discovery of *FOXO1* and *MYC* F153L mutation, likely valid mutations from duplex support and high VAF levels, suggests ctDNA can provide more information on clonal structure without guidance from mutation data of tumour biopsies. It is uncertain why these mutations were not detected in the tumour biopsy. Possible explanations include the limitations of tumour biopsies on assessing spatial heterogeneity, or the sequencing depth from WES of the tumour was not sufficient to identify these mutations. Regardless, this data suggest the sub-clones associated with *FOXO1* and *MYC* F153L mutation likely expanded during treatment resulting in disease progression in the patient. PT07 was not a discordant patient, however, ctDNA analysis concluded this patient had an insignificant decrease in mean VAF despite categorized as a non-responder. We discovered a valid novel variant in *MLL2* that increased in VAF, potentially associated with a sub-clone expansion that may explain treatment response in this patient, in a similar manner to PT11.

Novel variant discovery also holds promise for detecting variants in ctDNA when a tumour biopsy is unavailable to provide data for predictive target mutations. I performed numerous experiments to test this, however most cases had undetectable ctDNA or the filtering step failed to remove sequencing artifacts and false positives. Nevertheless, I have shown in this project that ctDNA can provide a suitable alternative to tumour biopsies for use in monitoring disease progression. However, there is a need

for robust software capable of utilizing sequence analysis from ctDNA in the absence of tumour samples. This has been demonstrated in our lab, where an alternative analysis methodology successfully detected real variants in plasma samples without a corresponding tumour sample (Geneious). The limitation of this methodology is the requirement of iterative, manual curation and an experienced user.

It is likely that some of the non-responding patients with significant ctDNA decreases correspond to examples of initial responses followed by resistance, as discussed in Chapter 2. Despite this, the discordant result of PT11 may be better explained by clonal evolution. The tumour population may comprise many clones or different sub-clones initially driving disease progression, however, treatment can successfully eliminate many of these sub-clones. If at least one sub-clone population survives treatment to drive relapse, the overall mean VAF may still decrease due to the decline of numerous sub-clones. Comprehensive analysis of ctDNA is necessary to determine the full extent of tumour heterogeneity in a patient and its evolution during treatment. As we have recently demonstrated in patients having undergone prior therapies, treatment resistance can involve outgrowth of a sub-clone that may be genetically related to the initial cancer but with an incomplete overlap in mutations. Such processes may likely explain why some patients showed apparently reduced ctDNA but ultimately relapsed. Detection of separate sub-clonal populations may well be achieved by performing targeted or global sequencing on additional plasma samples using methods utilized herein or, given the high level of ctDNA (in some cases approaching the level of tumour DNA present in tissue biopsies), using global strategies such as whole exome sequencing for unbiased mutation discovery in plasma.

Chapter 4.   Conclusions and Future Directions

4.1. Overall Conclusions

4.1.1. Utility of circulating tumour DNA as a biomarker on therapy

Throughout this work, I consistently found the hybridization-capture strategy to be more effective at detecting and accurately quantifying ctDNA. Overall, 90.9% of samples tested had ctDNA levels detectable with this method. Error suppression from molecular barcoding enabled single molecule identification and removed the requirement for a 1% VAF threshold. As VAFs for ctDNA can be low, especially in certain NHLs, error suppression allowed for sensitive detection, in some cases with single digit molecule counts (collapsed reads) of ctDNA in a background of hundreds of wildtype molecules. I conclude from this that, if relying only on the amplicon-based approach, we would be unable to use ctDNA as a biomarker in cases with limiting amounts of ctDNA (i.e. below 1%). Furthermore, error suppression removes false positives that may be called when detecting novel variants not observed in the tumour tissue.

Based on a limited number of patients, I found that ctDNA can be a useful biomarker for evaluating treatment response and disease progression. Specifically, 9 out of 13 non-responders from the QCROC cohort had significant increase in ctDNA after 15 days. Including the four non-responders with detectable ctDNA presented in Chapter 3 (PT255, PT419, BC02 and BC12), we conclude 13 of 17 non-responding patients showed significant increase in ctDNA.

An increase in ctDNA can thus be considered a biomarker to monitor treatment response. As a clinical test, this metric would have a PPV of 100% because every patient reported with a significant increase had responded poorly to treatment. This is clinically relevant, as it implies that the first sign of an increase in ctDNA ultimately indicates the patient will likely respond poorly to treatment. A significantly larger number of patients would be needed to evaluate the generalizability of this observation.

4.1.2. Utility of circulating tumour DNA to inform on tumour heterogeneity and evolution

For ctDNA to be applied in clinical settings as an adjunct to (or replacement for) tumour tissue biopsies, we need to determine its utility to capture the mutations present in a tissue biopsy while also informing on tumour heterogeneity that is not well represented in a single tissue sample. Although the VAF of mutations in ctDNA is much lower than in tumour biopsies, improvements in detection sensitivity such as single molecule identification in hybridization capture, allow for low VAF mutations to be represented. In several patients, I demonstrated that ctDNA can accurately represent the landscape of mutations observed in tumour samples. The results from these experiments also supported the utility of ctDNA to inform on spatial heterogeneity, however further testing of this is needed.

I have shown the utility of ctDNA to inform on temporal ITH when testing sequentially obtained plasma samples during the course of treatment. From this, and other experiments on NHL patients, I have shown the potential for ctDNA to inform on the clonal structure of a tumour. I was able to distinguish sub-clones by tracking different mutations affecting the same gene, which appear to have arisen in a process of convergent evolution. Analysis of these mutations through several time points provided insight on how the sub-clonal structure evolved in these patients during treatment.

4.2. Future Directions

4.2.1. Continued plasma time point analysis on BCCA cohort using improved hybridization capture techniques

The collection of plasma for the patients from the BCCA cohort is ongoing. These plasma samples follow a scheduled time course, with any progression in disease clinically reported. Hybridization capture or exome capture on these plasma samples can be performed in a similar experiment to the QCROC cohort. Future experiments should include a greater amount of template cfDNA (at least 100 ng of input) to increase the LOD, as the plasma samples from these patients are not a limiting factor. These experiments will provide more evidence and support to the utility of ctDNA to inform on treatment response and disease progression. Patients from this cohort regularly have

blood collected, but do not regularly have tumour biopsies obtained. Thus, the sub-clonal structure in the tumours may have changed compared to the most recent tumour biopsy. WES should be performed on these plasma samples, followed by analysis for novel variants to assess potential mutations associated with a sub-clone previously unobserved through biopsies.

Future experiments should also use the improved custom adapters for hybridization capture. The five bp degenerate barcode has been extended to twelve bp, although only the first nine bases are used to identify cfDNA molecules, as we found the last three bases of the barcode were not reliable sequenced. Nevertheless, this provides an improved potential of 262,144 barcode permutations ($2^{(9+9)}$). The three bp fixed tag has been modified to be strand-specific and non-complementary, to provide a "bubble" between the degenerate barcode and the Illumina adapter sequence which provides improved annealing efficiency. Different sets of custom adapters were designed to contain unique three bp "sample specific" tags to provide another level of sample identification. Additionally, more xGen Lockdown® probes have been designed, which increases our capture space to include 73 lymphoma genes.

4.2.2. ProDuSe re-development for future analyses

The initial implementation of ProDuSe had numerous issues. One issue with the version of ProDuSe used for this project was the high number of sequence artifacts reported despite filtering variants, which resulted in laborious, manual curation. Another graduate student in the Morin lab is re-designing the software to address the known limitations. The new version is being designed to report indels and will have improved ability for detecting novel variants. For future clinical studies, having a tool such as ProDuSe can provide quick, comprehensive ctDNA analysis which may inform on treatment response. Additionally, using ProDuSe to detect novel variants in ctDNA may provide an alternative method for detecting new sub-clone outgrowths, which does not rely on invasive tumour tissue biopsies for continued monitoring of disease. It is advisable that raw and collapsed data from our QCROC cohort is eventually re-analyzed for novel variants by the newly re-designed ProDuSe.

4.2.3. Single cell validation experiments

Although convergent evolution towards mutations in the same gene allowed us to identify changes in the sub-clonal population of a tumour, this is not applicable in all patients. In cases where we cannot assume that a mutation is associated with a certain sub-clone, we will need further experiments to test the clonal structure of a tumour. Multiplexed, single-cell experiments for mutation analysis provide a method to examine the sub-clonal architecture[124]. This has been performed in breast cancer experiments[125] and acute lymphoblastic leukemia experiments[126], however no study has been done in lymphoma to date. Another graduate student in our lab performed single cell experiments on PT255 to confirm the results from our ctDNA analysis (not included in this project). By separating tumour samples into single cells, and then performing amplicon sequencing on each individual cell, we can decisively determine if a mutation is associated with a certain sub-clone. The results from the single cell experiments on PT255 confirmed that the presence of two sub-clones. For future experiments that discover potential sub-clonal population of tumour cells, single cell validation experiments are required to confirm the results.

References

1. Canadian Cancer Society's Advisory Committee on Cancer Statistics. Canadian Cancer Statistics 2017. *Can. Cancer Soc.* 1–132 (2017).

2. Canadian Cancer Society/National Cancer Institute of Canada. Canadian Cancer Statistics 2005. *Can. Cancer Soc.* 1–110 (2005).

3. Sudhakar, A. History of Cancer, Ancient and Modern Treatment Methods. *J Cancer Sci Ther.* **1,** 1–4 (2010).

4. Stratton, K., Shetty, P., Wallace, R. & Bondurant, S. Clearing the smoke: the science base for tobacco harm reduction. *Tob. Control* **10,** 189–95 (2001).

5. Boveri, T. Concerning the Origin of Malignant Tumours by Theodor Boveri. Translated and annotated by Henry Harris. *J. Cell Sci.* **121,** 1–84 (2008).

6. Yamagiwa, K. & Ichikawa, K. Experimental Study of the Pathogenesis of Carcinoma. *J. Cancer Res.* **3,** 1–29 (1918).

7. Nowell, P. C. & Hungerford, D. A. Chromosome Studies in Human Leukemia. II. Chronic Granulocytic Leukemia. *J. Natl. Cancer Inst.* **27,** 1013–1035 (1961).

8. Stratton, M. R., Campbell, P. J. & Futreal, P. A. The cancer genome. *Nature* **458,** 719–724 (2009).

9. Vogelstein, B. & Kinzler, K. W. The multistep nature of cancer. *Trends in Genetics* **9,** 138–141 (1993).

10. Pleasance, E. D. *et al.* A comprehensive catalogue of somatic mutations from a human cancer genome. *Nature* **463,** 191–196 (2010).

11. Loeb, L. A. & Harris, C. C. Advances in Chemical Carcinogenesis: A Historical Review and Prospective. *Cancer Res.* **68,** 6863–6872 (2008).

12. Greenman, C. *et al.* Patterns of somatic mutation in human cancer genomes. *Nature* **446,** 153–158 (2007).

13. Martinocorena, I. & Campbell, P. J. Somatic mutation in cancer and normal cells. *Science (80-.).* **349,** 1483–1489 (2015).

14. Merlo, L. M. F., Pepper, J. W., Reid, B. J. & Maley, C. C. Cancer as an evolutionary and ecological process. *Nat. Rev. Cancer* **6,** 924–935 (2006).

15. Levine, A. J., Hu, W. & Feng, Z. *The Molecular Basis of Cancer 3rd Edition.* (Elsevier Inc., 2008). doi:10.1016/B978-141603703-3.10064-0

16. Knudson, A. G. Mutation and Cancer: Statistical Study of Retinoblastoma. *Proc. Natl. Acad. Sci.* **68,** 820–823 (1971).

17. Marusyk, A. & Polyak, K. Tumor heterogeneity: causes and consequences. *Biochim Biophys Acta* **1805,** 1–28 (2011).

18. Bonnet, D. & Dick, J. E. Human acute myeloid leukemia is organized as a hierarchy that originates from a primitive hematopoietic cell. *Nat. Med.* **3,** 730–737 (1997).

19. Beck, B. & Blanpain, C. Unravelling cancer stem cell potential. *Nat. Rev. Cancer* **13,** 727–738 (2013).

20. Bruce, W. R. & Van Der Gaag, H. A quantitative assay for the number of murine lymphoma cells capable of proliferation in vivo. *Nature* **199,** 79–80 (1963).

21. Martinez-Climent, J. A., Fontan, L., Gascoyne, R. D., Siebert, R. & Prosper, F. Lymphoma stem cells: Enough evidence to support their existence? *Haematologica* **95,** 293–302 (2010).

22. Kim, S. J. Lymphoma stem cells: A step toward a new therapeutic target. *Korean J. Hematol.* **46,** 211 (2011).

23. Okosun, J. *et al.* Integrated genomic analysis identifies recurrent mutations and evolution patterns driving the initiation and progression of follicular lymphoma. *Nat. Genet.* **46,** 176–181 (2014).

24. Devarakonda, S. & Govindan, R. Clonal evolution: Multiregion sequencing of esophageal adenocarcinoma before and after chemotherapy. *Cancer Discov.* **5,** 796–798 (2015).

25. Cairns, J. Mutation selection and the natural history of cancer. *Nature* **255,** 197–200 (1975).

26. Nowell, P. C. The clonal evolution of tumor cell populations. *Science (80-.).* **194,** 23–28 (1976).

27. Davis, A., Gao, R. & Navin, N. Tumor evolution: Linear, branching, neutral or punctuated? *Biochim. Biophys. Acta - Rev. Cancer* **1867,** 151–161 (2017).

28. Fearon, E. R. & Vogelstein, B. A genetic model for colorectal tumorigenesis. *Cell* **61,** 759–767 (1990).

29. Gawad, C., Koh, W. & Quake, S. R. Dissecting the clonal origins of childhood acute lymphoblastic leukemia by single-cell genomics. *Proc. Natl. Acad. Sci.* **111,** 17947–17952 (2014).

30. Vogelstein, B. *et al.* Cancer Genome Landscapes. *Science (80-.).* **339,** 1546–

1558 (2013).

31.   McGranahan, N. & Swanton, C. Clonal Heterogeneity and Tumor Evolution: Past, Present, and the Future. *Cell* **168,** 613–628 (2017).

32.   Cusnir, M. & Cavalcante, L. Inter-tumor heterogeneity. *Hum. Vaccin. Immunother.* **8,** 1143–1145 (2012).

33.   Burrell, R. A., McGranahan, N., Bartek, J. & Swanton, C. The causes and consequences of genetic heterogeneity in cancer evolution. *Nature* **501,** 338–345 (2013).

34.   Lennert, K. *Malignant Lymphomas Other than Hodgkin's Disease.* (Springer-Verlag Berlin Heidelberg, 1978). doi:10.1007/978-3-642-81092-3

35.   Küppers, R. & Rajewsky, K. The Origin of Hodgkin and Reed/Sternberg Cells in Hodgkin's Disease. *Annu. Rev. Immunol.* **16,** 471–493 (1998).

36.   Martelli, M. *et al.* Diffuse large B-cell lymphoma. *Crit. Rev. Oncol. Hematol.* **87,** 146–171 (2013).

37.   Smith, S. D. *et al.* Comparison of outcomes after auto-SCT for patients with relapsed diffuse large B-cell lymphoma according to previous therapy with rituximab. *Bone Marrow Transplant.* **46,** 262–266 (2011).

38.   Alizadeh, A. A. *et al.* Distinct types of diffuse large B-cell lymphoma identified by gene expression profiling. *Nature* **403,** 503–511 (2000).

39.   Rosenwald, A. & Staudt, L. Gene expression profiling of diffuse large B-cell lymphoma. *Leuk lymphoma* **44 Suppl 3,** S41-47 (2003).

40.   Pasqualucci, L. & Dalla-Favera, R. The Genetic Landscape of Diffuse Large B cell Lymphoma. *Semin Hematol* **52,** 67–76 (2015).

41.   Lenz, G. & Staudt, L. M. Aggressive lymphomas. *N Engl J Med* **362,** 1417–1429 (2010).

42.   Lenz, G. *et al.* Molecular subtypes of diffuse large B-cell lymphoma arise by distinct genetic pathways. *Proc Natl Acad Sci USA* **105,** 13520–13525 (2008).

43.   Morin, R. D. *et al.* Somatic mutation of EZH2 (Y641) in Follicular and Diffuse Large B-cell Lymphomas of Germinal Center Origin. *Nat. Genet.* **42,** 181–185 (2010).

44.   Morin, R. D. *et al.* Frequent mutation of histone-modifying genes in non-Hodgkin lymphoma. *Nature* **476,** 298–303 (2011).

45.   Pasqualucci, L. *et al.* Inactivating mutations of acetyltransferase genes in B-cell

lymphoma. *Nature* **471,** 189–195 (2011).

46. The Non-Hodgkin's Lymphoma Classification Project. A Clinical Evaluation of the International Lymphoma Study Group Classification of Non-Hodgkin's Lymphoma. *Blood* **89,** 3909–3918 (1997).

47. Kridel, R., Sehn, L. H. & Gascoyne, R. D. Review series Pathogenesis of follicular lymphoma. *J. Clin. Invest.* **122,** 3424–3431 (2012).

48. O'Shea, D. *et al.* The presence of TP53 mutation at diagnosis of Follicular Lymphoma identifies a high-risk group of patients with shortened time to disease progression and poorer overall survival. *Blood* **112,** 3126–3129 (2008).

49. Luminari, S. & Federico, M. Prognosis of follicular lymphomas. *Hematol. Oncol.* **24,** 64–72 (2006).

50. Montoto, S. *et al.* Risk and clinical implications of transformation of follicular lymphoma to diffuse large B-cell lymphoma. *J. Clin. Oncol.* **25,** 2426–2433 (2007).

51. Casulo, C., Burack, W. R. & Friedberg, J. W. Transformed follicular non-Hodgkin lymphoma. *Blood* **125,** 40–47 (2015).

52. Roschewski, M., Staudt, L. M. & Wilson, W. H. Diffuse large B-cell lymphoma—treatment approaches in the molecular era. *Nat. Rev. Clin. Oncol.* **11,** 12–23 (2013).

53. Vaidya, R. & Witzig, T. E. Prognostic factors for diffuse large B-cell lymphoma in the R(X)CHOP era. *Ann. Oncol.* **25,** 2124–2133 (2014).

54. Guirguis, H. R. *et al.* Survival of patients with transformed lymphoma in the rituximab era. *Ann. Hematol.* **93,** 1007–1014 (2014).

55. Maloney, D. G. *et al.* Phase I clinical trial using escalating single-dose infusion of chimeric anti-CD20 monoclonal antibody (IDEC-C2B8) in patients with recurrent B-cell lymphoma. *Blood* **84,** 2457–2466 (1994).

56. Rudnicka, D. *et al.* Rituximab causes a polarization of B cells that augments its therapeutic function in NK-cell–mediated antibody-dependent cellular cytotoxicity. *Blood* **121,** 4694–4702 (2013).

57. Hall, A. G. & Tilby, M. J. Mechanisms of action of, and modes of resistance to, alkylating agents used in the treatment of haematological malignancies. *Blood Rev.* **6,** 163–173 (1992).

58. Tacar, O., Sriamornsak, P. & Dass, C. R. Doxorubicin: An update on anticancer molecular action, toxicity and novel drug delivery systems. *Journal of Pharmacy and Pharmacology* **65,** 157–170 (2013).

59.   Jordan, M. Mechanism of Action of Antitumor Drugs that Interact with Microtubules and Tubulin. *Curr. Med. Chem. Agents* **2,** 1–17 (2012).

60.   Récher, C. *et al.* Intensified chemotherapy with ACVBP plus rituximab versus standard CHOP plus rituximab for the treatment of diffuse large B-cell lymphoma (LNH03-2B): An open-label randomised phase 3 trial. *Lancet* **378,** 1858–1867 (2011).

61.   Dunleavy, K. *et al.* Dose-Adjusted EPOCH-Rituximab Therapy in Primary Mediastinal B-Cell Lymphoma. *N. Engl. J. Med.* **368,** 1408–1416 (2013).

62.   Pommier, Y., Leo, E., Zhang, H. & Marchand, C. DNA topoisomerases and their poisoning by anticancer and antibacterial drugs. *Chemistry and Biology* **17,** 421–433 (2010).

63.   Tilly, H. *et al.* Intensive conventional chemotherapy (ACVBP regimen) compared with standard CHOP for poor-prognosis aggressive non-Hodgkin lymphoma. *Blood* **102,** 4284–4289 (2003).

64.   Seidel, M. G. Autoimmune and other cytopenias in primary immunodeficiencies: Pathomechanisms, novel differential diagnoses, and treatment. *Blood* **124,** 2337–2344 (2014).

65.   Hong, J. *et al.* Anemia as a useful biomarker in patients with diffuse large B-cell lymphoma treated with R-CHOP immunochemotherapy. *Cancer Sci.* **105,** 1569–1575 (2014).

66.   Park, S. *et al.* Clinical significance of non-neutropenic fever in the management of diffuse large B-cell lymphoma patients treated with rituximab-CHOP: Comparison with febrile neutropenia and risk factor analysis. *Cancer Res. Treat.* **47,** 448–457 (2015).

67.   El-Osta, H. & Nair, B. Rituximab-induced acute thrombocytopenia: An underappreciated entity. *Leukemia and Lymphoma* **54,** 2736–2737 (2013).

68.   Nagashima, K., Tanaka, H., Nagai, Y. & Sugita, Y. Immune pancytopenia after chemotherapy in a patient with diffuse large B-cell lymphoma. *BMJ Case Rep.* (2016). doi:10.1136/bcr-2016-216880

69.   Wahaib, K., Beggs, A. E., Campbell, H., Kodali, L. & Ford, P. D. Panobinostat: A histone deacetylase inhibitor for the treatment of relapsed or refractory multiple myeloma. *Am. J. Heal. Pharm.* **73,** 441–450 (2016).

70.   McCabe, M. T. *et al.* EZH2 inhibition as a therapeutic strategy for lymphoma with EZH2-activating mutations. *Nature* **492,** 108–112 (2012).

71.   Qi, W. *et al.* Selective inhibition of Ezh2 by a small molecule inhibitor blocks tumor cells proliferation. *Proc. Natl. Acad. Sci.* **109,** 21360–21365 (2012).

72.   Sklair-Levy, M. *et al.* Image-guided cutting-edge-needle biopsy of peripheral lymph nodes and superficial masses for the diagnosis of lymphoma. *J. Comput. Assist. Tomogr.* **29,** 369–372 (2005).

73.   Buchpiguel, C. A. Current status of PET/CT in the diagnosis and follow up of lymphomas. *Rev. Bras. Hematol. Hemoter.* **33,** 140–147 (2011).

74.   Herman, G. *Fundamentals of Computerized Tomography 2nd Edition.* (Springer-Verlag London, 2009). doi:10.1007/978-1-84628-723-7

75.   Friedberg, J. W. & Chengazi, V. PET scans in the staging of lymphoma: current status. *Oncologist* **8,** 438–447 (2003).

76.   Johnson, S. A., Kumar, A., Matasar, M. J., Schöder, H. & Rademaker, J. Imaging for Staging and Response Assessment in Lymphoma. *Radiology* **276,** 323–338 (2015).

77.   Frampas, E. Lymphomas: Basic points that radiologists should know. *Diagn. Interv. Imaging* **94,** 131–144 (2013).

78.   Chien, S. H. *et al.* Frequency of surveillance computed tomography in non-Hodgkin lymphoma and the risk of secondary primary malignancies: A nationwide population-based study. *Int. J. Cancer* **137,** 658–665 (2015).

79.   Graña, L., Calzado, A., Hernández, P. & Rodríguez, R. Role of computed tomography on large B-cell non-Hodgkin's lymphoma follow-up and the risk of radiation-induced neoplasm: A retrospective cohort study. *Eur. J. Radiol.* **85,** 673–679 (2016).

80.   El-Galaly, T. C. *et al.* Routine imaging for diffuse large b-cell lymphoma in first complete remission does not improve post-treatment survival: A danishâ€"swedish population-based study. *J. Clin. Oncol.* **33,** 3993–3998 (2015).

81.   Paolicchi, F. *et al.* Radiation dose exposure in patients affected by lymphoma undergoing repeat CT examinations: how to manage the radiation dose variability. *Radiol. Medica* **123,** 191–201 (2018).

82.   National Guideline Alliance (UK). *Non-Hodgkin's Lymphoma: Diagnosis and Management.* (London: National Institute for Health and Care Excellence (UK), 2016).

83.   Yadav, C. *et al.* Serum Lactate Dehydrogenase in Non-Hodgkin's Lymphoma: A Prognostic Indicator. *Indian J. Clin. Biochem.* **31,** 240–242 (2016).

84.   Fasola, G. *et al.* Serum LDH concentration in non-Hodgkin's lymphomas. Relationship to histologic type, tumor mass, and presentation features. *Acta Haematol.* **72,** 231–238 (1984).

85. Endrizzi, L. *et al.* Serum lactate dehydrogenase (LDH) as a prognostic index for non-Hodgkin's lymphoma. *Eur. J. Cancer Clin. Oncol.* **18,** 945–949 (1982).

86. Pepe, M. S. *et al.* Phases of Biomarker Development for Early Detection of Cancer. *Cancer* **93,** 1054–1061 (2001).

87. Alix-Panabières, C., Schwarzenbach, H. & Pantel, K. Circulating tumor cells and circulating tumor DNA. *Annu. Rev. Med.* **63,** 199–215 (2012).

88. Mouliere, F. *et al.* High fragmentation characterizes tumour-derived circulating DNA. *PLoS One* **6,** 1–10 (2011).

89. Schwarzenbach, H., Hoon, D. S. B. & Pantel, K. Cell-free nucleic acids as biomarkers in cancer patients. *Nature Reviews Cancer* **11,** 426–437 (2011).

90. Leon, S. A. *et al.* Free DNA in the Serum of Cancer Patients and the Effect of Therapy Free DNA in the Serum of Cancer Patients and the Effect of Therapy. *Cancer Res* **37,** 646–650 (1977).

91. Diehl, F. *et al.* Circulating mutant DNA to assess tumor dynamics. *Nat. Med.* **14,** 985–990 (2008).

92. Leung, F. *et al.* Circulating Tumor DNA as a Cancer Biomarker: Fact or Fiction? *Clin. Chem.* **62,** 1054–1060 (2017).

93. Mäbert, K. *et al.* Cancer biomarker discovery: Current status and future perspectives. *Int. J. Radiat. Biol.* **90,** 659–677 (2014).

94. Cristofanilli, M. *et al.* Circulating Tumor Cells, Disease Progression, and Survival in Metastatic Breast Cancer. *N. Engl. J. Med.* **351,** 781–791 (2004).

95. Pantel, K. & Brakenhoff, R. H. Dissecting the metastatic cascade. *Nat. Rev. Cancer* **4,** 448–456 (2004).

96. Wiernik, P. H. Serum CA125 and PSA concentrations in patients with lymphoma. *Clin Adv Hematol Oncol* **6,** 527–531 (2008).

97. Saouli, Z. *et al.* Tumor Marker CA 15-3 in Hematological Malignancies. *Blood* **108,** (2006).

98. Diaz, L. A. & Bardelli, A. Liquid biopsies: Genotyping circulating tumor DNA. *J. Clin. Oncol.* **32,** 579–586 (2014).

99. Gingras, I., Salgado, R. & Ignatiadis, M. Liquid biopsy. *Curr. Opin. Oncol.* **27,** 560–567 (2015).

100. Armand, P. *et al.* Detection of circulating tumour DNA in patients with aggressive B-cell non-Hodgkin lymphoma. *Br. J. Haematol.* **163,** 123–126 (2013).

101. Dawson, S. *et al.* Analysis of Circulating Tumor DNA to Monitor Metastatic Breast Cancer. *N. Engl. J. Med.* **368,** 1199–1209 (2013).

102. Bettegowda, C. *et al.* Detection of Circulating Tumor DNA in Early- and Late-Stage Human Malignancies. *Sci. Transl. Med.* **6,** 1–11 (2014).

103. Crowley, E., Di Nicolantonio, F., Loupakis, F. & Bardelli, A. Liquid biopsy: monitoring cancer-genetics in the blood. *Nat. Rev. Clin. Oncol.* **10,** 472–484 (2013).

104. Heitzer, E., Perakis, S., Geigl, J. B. & Speicher, M. R. The potential of liquid biopsies for the early detection of cancer. *npj Precis. Oncol.* **1,** 36 (2017).

105. Almendro, V., Marusyk, A. & Polyak, K. Cellular Heterogeneity and Molecular Evolution in Cancer. *Annu. Rev. Pathol. Mech. Dis.* **8,** 277–302 (2013).

106. Gerlinger, M. *et al.* Intratumor heterogeneity and branched evolution revealed by multiregion sequencing. *N Engl J Med* **366,** 883–892 (2012).

107. Shendure, J. & Ji, H. Next-generation DNA sequencing. *Nat. Biotechnol.* **26,** 1135–1145 (2008).

108. Hodkinson, B. P. & Grice, E. A. Next-Generation Sequencing: A Review of Technologies and Tools for Wound Microbiome Research. *Adv. Wound Care* **4,** 50–58 (2015).

109. Fedurco, M., Romieu, A., Williams, S., Lawrence, I. & Turcatti, G. BTA, a novel reagent for DNA attachment on glass and efficient generation of solid-phase amplified DNA colonies. *Nucleic Acids Res.* **34,** 1–13 (2006).

110. Canard, B. & Sarfati, R. S. DNA polymerase fluorescent substrates with reversible 3′-tags. *Gene* **148,** 1–6 (1994).

111. Turcatti, G., Romieu, A., Fedurco, M. & Tairi, A. P. A new class of cleavable fluorescent nucleotides: Synthesis and optimization as reversible terminators for DNA sequencing by synthesis. *Nucleic Acids Res.* **36,** (2008).

112. Knief, C. Analysis of plant microbe interactions in the era of next generation sequencing technologies. *Front. Plant Sci.* **5,** 1–23 (2014).

113. Quail, M. A. *et al.* A tale of three next generation sequencing platforms: comparison of Ion Torrent, Pacific Biosciences and Illumina MiSeq sequencers. *BMC Genomics* **13,** 1–13 (2012).

114. Schmitt, M. W. *et al.* Detection of ultra-rare mutations by next-generation sequencing. *Proc. Natl. Acad. Sci.* **109,** 14508–14513 (2012).

115. Kennedy, S. R. *et al.* Detecting ultralow-frequency mutations by Duplex

Sequencing. *Nat. Protoc.* **9,** 2586–2606 (2014).

116. Han, X., Wang, J. & Sun, Y. Circulating Tumor DNA as Biomarkers for Cancer Detection. *Genomics, Proteomics Bioinforma.* **15,** 59–72 (2017).

117. Newman, A. M. *et al.* An ultrasensitive method for quantitating circulating tumor DNA with broad patient coverage. *Nat. Med.* **20,** 548–554 (2014).

118. Malapelle, U. *et al.* Next generation sequencing techniques in liquid biopsy: focus on non-small cell lung cancer patients. *Transl. Lung Cancer Res.* **5,** 505–510 (2016).

119. Shu, Y. *et al.* Circulating Tumor DNA Mutation Profiling by Targeted Next Generation Sequencing Provides Guidance for Personalized Treatments in Multiple Cancer Types. *Sci. Rep.* **7,** 1–11 (2017).

120. Fan, H. C., Blumenfeld, Y. J., Chitkara, U., Hudgins, L. & Quake, S. R. Noninvasive diagnosis of fetal aneuploidy by shotgun sequencing DNA from maternal blood. *PNAS* **105,** 1–6 (2008).

121. Medina Diaz, I. *et al.* Performance of Streck cfDNA blood collection tubes for liquid biopsy testing. *PLoS One* **11,** 1–18 (2016).

122. Roschewski, M., Staudt, L. M. & Wilson, W. H. Dynamic monitoring of circulating tumor DNA in non-Hodgkin lymphoma. *Blood* **127,** 3127–3132 (2016).

123. Johnson, N. A. *et al.* CD20 mutations involving the rituximab epitope are rare in diffuse large B-cell lymphomas and are not a significant cause of R-CHOP failure. *Haematologica* **94,** 423–427 (2009).

124. Greaves, M. & Maley, C. C. Clonal evolution in cancer. *Nature* **481,** 306–313 (2012).

125. Navin, N. *et al.* Tumour evolution inferred by single-cell sequencing. *Nature* **472,** 90–94 (2011).

126. Anderson, K. *et al.* Genetic variegation of clonal architecture and propagating cells in leukaemia. *Nature* **469,** 356–361 (2011).